CeO_2 and La_2O_3 promoters in the steam reforming of polyolefinic waste plastic pyrolysis volatiles on Ni-based catalysts

Aitor Arregi[a], Mehrdad Seifali Abbas-Abadi[b], Gartzen Lopez[a,c*], Laura Santamaria[a], Maite Artetxe[a], Javier Bilbao[a] and Martin Olazar[a]

[a]Department of Chemical Engineering, University of the Basque Country UPV/EHU, P.O. Box 644 - E48080 Bilbao (Spain), gartzen.lopez@ehu.es

[b]Laboratory for Chemical Technology, Department of Materials, Textiles and Chemical Engineering, Faculty of Engineering & Architecture, Ghent University, Technologiepark 914, B-9052 Zwijnaarde, Belgium

[c]IKERBASQUE, Basque Foundation for Science, Bilbao, Spain

Abstract

Based on the promising results of La_2O_3 and CeO_2 promoted Ni/Al_2O_3 catalysts in the reforming of biomass pyrolysis volatiles, the performance of these catalysts and the non-promoted one was

evaluated in the pyrolysis and in-line steam reforming of polypropylene (PP). The experiments were carried out in a continuous bench scale pyrolysis-reforming plant using two space times of 4.1 and 16.7 g_{cat} min $g_{plastic}^{-1}$ and a steam/PP ratio of 4. The prepared catalysts and the deposited coke were characterized by N_2 adsorption-desorption, X-ray fluorescence (XRF), X-ray diffraction (XRD), temperature programmed oxidation (TPO) and transmission electron microscopy (TEM). The Ni/Al_2O_3 catalyst showed suitable performance regarding pyrolysis product conversion and hydrogen production, and led to moderate coke deposition. It is to note that La_2O_3 incorporation remarkably improved catalyst performance compared to the other two catalysts in terms of conversion (> 99 %), hydrogen production (34.9 %) and coke deposition (2.24 wt%).

Keywords: Hydrogen; Pyrolysis; Reforming; Waste plastics; La_2O_3 ; CeO_2; Deactivation; Coke.

Introduction

Polymers with their unrivaled properties and low cost are now replacing the natural and mineral resources such as stone, wood, paper, metal, glass, wool, leather, and so on, and their consumption and applications, as well as the amount of wastes they generate, are increasing rapidly [1]. Moreover, landfill and incineration, which are at present the main ways for non-recyclable polymeric waste disposal, are no longer suitable environmental solutions [2].

Furthermore, polyolefin polymers (mainly polyethylene and polypropylene) remain in the environment for many years, longer than other plastics due to the absence of a functional group recognizable by soil enzymes. Pyrolysis and liquefaction for the production of valuable fuels can be suitable solutions for the upgrading of polymer wastes, which have received great attention in recent years [3-7]. Moreover, steam gasification of waste plastics has been proposed for the production of hydrogen rich gas [8-12]. More recently, pyrolysis-reforming has also been demonstrated to be especially suitable for the selective production of hydrogen from waste plastics [13-22].

In the steam reforming process, steam is an active carrier gas that reacts with the feed into the reformer, i.e., part of the hydrogen produced comes from that contained in the steam. Hydrogen production by means of steam reforming from waste polymers can be accomplished following two main strategies: (i) in-situ gasification with a reforming catalyst and (ii) pyrolysis and in-line reforming of the volatile stream leaving the pyrolysis reactor. However, the first strategy requires more energy, as process temperatures are higher [23]. In addition, mineral and metal additives in plastics inactivate catalysts more rapidly by making them more difficult to recover and reuse [23-26]. Polyolefins have higher hydrogen content compared to other plastics, such as polystyrene or polyethylene terephthalate, and specifically higher than biomass. Accordingly, higher hydrogen yields have been reported in the pyrolysis-reforming of polyolefins in relation to the mentioned feedstocks [13, 14, 27-31]. Moreover, the composition of the pyrolysis products obtained in polyolefin pyrolysis, mainly waxes and other paraffinic and olefinic compounds,

attenuate coke deposition, as their potential to deactivate the catalyst is lower than those oxygenates formed in biomass pyrolysis [31] or aromatic compounds in the pyrolysis of other waste plastics [26, 28, 32]. In spite of the suitable characteristics of polyolefins for their valorization by pyrolysis-reforming, the development of highly active and stable catalysts means a bottleneck for the scale up of the process.

The features of the support greatly influence catalyst activity and stability. In fact, a suitable support should provide high surface area and suitable pore distribution, as well as a strong metal-support interaction, adequate mechanical strength and thermal stability. A wide variety of supports have been used in the reforming of both biomass and plastics pyrolysis products, with metal oxides [33-36], zeolites[19, 37, 38] and activated carbon [14, 39] being the most widely reported supports. It is to note that alumina is a material of high chemical and mechanical resistance, low cost and high surface area for metal dispersion, and has therefore been widely used as a support in the reforming industry [40]. In addition, Ni, Ru, Pt and Fe have been used as metallic phases in catalysts for hydrogen production in the reforming of biomass and waste derived products [41]. Compared to the other metals studied, catalysts based on Ni combine high activity for breaking C-C and C-H bonds with relatively moderate cost, and are therefore the preferred choice for the reforming process [40, 42-45]. Accordingly, Ni supported on Al_2O_3 catalyst is one of the most widely used in the field of steam reforming and hydrogen production [46, 47].

However, most the catalysts studied in the reforming of biomass and waste derived products undergo a severe coke deposition with a fast deactivation rate. Specifically, coke deposition on Ni/Al_2O_3 catalysts is enhanced by Al_2O_3 acidity [40, 48]. Previous research has shown that catalysts promoted with specific metals and metal oxides, such as Ce, Mg, La and Zr, have higher stability and activity, resistance to deactivation (lower coke deposition) and higher ability for water adsorption/dissociation [49-52]. Although promoted catalysts have been commonly used in the reforming of biomass-derived volatiles, they have been hardly used utilization in the reforming of waste plastics. Thus, the research group headed by Prof. Williams has analyzed

different promoted catalysts, such as $Ni/CeO_2/Al_2O_3$, $Ni/MgO/Al_2O_3$ or Ni/CeO_2/ZSM-5, in the reforming of pyrolysis products from different plastics in a two fixed bed reactor system [24, 53-56].

This paper analyzes the performance of Ni/Al_2O_3 and two promoted catalysts (Ni/CeO_2-Al_2O_3 and Ni/La_2O_3-Al_2O_3) in the steam reforming of polypropylene derived volatiles using two space times. These promoted catalysts showed a promising performance in the reforming of biomass fast pyrolysis products in the same reaction unit [50, 57]. Fresh and used catalysts have been studied in detail in order to progress in the understanding of the reaction and deactivation mechanisms. The pyrolysis and in-line reforming runs were performed continuously using a conical spouted bed reactor (CSBR) for pyrolysis and a fluidized bed reactor (FBR) for reforming. This novel two reactor configuration combines the features of spouted beds for plastics fast pyrolysis and those of fluidized beds for the in-line catalytic steam reforming [16]. Thus, this system has been successfully applied for the pyrolysis-reforming of biomass, waste plastics and their mixtures [16, 31, 58].

Experimental

Materials

The polypropylene (PP) was purchased from Dow Chemical in the form of granules. The main specifications of the PP provided by the supplier are as follows: average molecular weight (M_w), 50-90 kg mol^{-1}; and polydispersity, 2.0. The higher heating value (HHV) of 44 MJ kg^{-1} has been determined using isoperibolic bomb calorimetry (Parr 1356) and differential scanning calorimetry (Setaram TG-DSC-111).

Catalysts synthesis and characterization

In this study, three custom-made catalysts prepared in the laboratory were used. The specifications of the catalysts are shown in Table 1. As usual, the calcination process at 1000 °C for 5 h under air atmosphere was used to pretreat γ-Al_2O_3 and drive off nearly all chemically combined water. The calcined support has great chemical purity, extreme hardness, high

density, good thermal conductivity and high electrical resistivity at high temperatures [59]. The calcined Al_2O_3 may stand phase changes during the process, and is therefore a suitable support to produce catalysts with high mechanical strength.

To prepare the Ni/Al_2O_3 catalyst, wet impregnation of the support with an aqueous solution of $Ni(NO_3)_2{\cdot}6H_2O$ *(VWR Chemicals,99%)* was used. After the impregnation process, the prepared catalyst was dried at 100 °C for 24 h and subsequently calcined at 700 °C for 3 h.

To produce the promoted catalysts of Ni/La_2O_3-Al_2O_3 and Ni/CeO_2-Al_2O_3, the preparation process of the Ni/Al_2O_3 catalyst should be modified. First, the promoted support was prepared by a subsequent wet impregnation method. To produce the Ni/La_2O_3-Al_2O_3 and Ni/CeO_2-Al_2O_3 catalysts, La_2O_3 and CeO_2 were loaded into the support prior to Ni in order to modify the Al_2O_3, following the impregnation method with aqueous solutions of $La(NO_3)_3{\cdot}6H_2O$ and $Ce(NO_3)_3.6H_2O$ *(VWR Chemicals, 99%),* respectively. The concentration of the metal promoter oxide (La_2O_3 or CeO_2) in the Al_2O_3 was fixed at 10 wt%. The support was dried overnight and calcined at 900 °C for 3 h. Afterwards, the support was impregnated with a Ni metal precursor ($Ni(NO_3)_2{\cdot}6H_2O$), dried at 100 ºC overnight and calcined at 700 ºC for 3 h. A nominal content of the metallic phase of 10 wt% was the target.

Catalyst characterization

Following Brunauer–Emmett–Teller (BET) methodology based on N_2 adsorption-desorption, a *Micromeritics ASAP 2010* instrument was used to determine the catalyst features, such as specific surface area and the properties of the porous structure (average pore size and pore volume). The sample was kept at 150 °C for 8 h to remove any impurity and degas it, and N_2 (99.9995 % purity) adsorption-desorption was then conducted in multiple equilibrium stages until saturation of the sample was achieved at cryogenic temperatures (liquid N_2).

To measure the metal (Ni, Ce and La) loaded into the prepared catalysts, X-ray fluorescence (XRF) spectrometry was used as an accurate measurement method. *PANalytical AXIOS* equipped with a Rh tube and three detectors (gaseous flow, scintillation and Xe sealing) was

used as a sequential wavelength dispersion X-ray fluorescence spectrometer to conduct chemical analysis under vacuum atmosphere.

The temperature programmed reduction (TPR) of the catalysts consisted in exposing the solid to a reducing gas flow, while a linearly increasing temperature sequence was maintained. To ascertain the reduction temperature of the different metallic phases in the catalyst, the H_2 consumed was monitored. A *Micromeritics AutoChem 2920* was used to carry out TPR. Thus, a flow of 10 vol% H_2/Ar circulated through the sample, which was heated with a constant heating rate of 5 °C min^{-1} from ambient temperature to 900 °C.

The crystalline structure of the fresh and deactivated catalysts was analyzed using X-ray powder diffraction (XRD) patterns. A *Bruker D8 Advance* diffractometer with $CuK_{\alpha 1}$ radiation was used to conduct XRD and the Scherrer formula was used to calculate the average Ni crystallite size. The device was equipped with a Bragg-Brentano geometry, Germanium primary monochromator, and a $CuK_{\alpha 1}$ wavelength of 1.5406 (Å), corresponding to an X-ray tube with Cu anticathode. Sol-X dispersive energy detector was employed, with a window optimized for $CuK_{\alpha 1}$ for limiting the fluorescence radiation. Continuous data collection was carried out from 10 to 80 °, with steps of 0.04 ° in 2θ, and measurement times per step of 12 s.

Total surface acidity of the catalysts was determined by NH_3-TPD runs in an *AutoChem II 2920 Micromeritics* equipment. The procedure entails the following steps: i) removal of the adsorbed volatile impurities with a He stream following a ramp of 15 °C min^{-1} to 550 °C; ii) adsorption of NH_3 (150 μL min^{-1}) until reaching sample saturation; (iii) desorption of the physisorbed NH_3 with a He stream at 150 °C, and (iv) desorption of the chemisorbed NH_3 at programmed temperature from 150 to 550 °C, with the TCD signal being recorded continuously.

The amount of coke deposited on the deactivated catalysts was determined by air combustion in a *TA Instruments TGA Q5000* thermogravimetric (TG) instrument, coupled in-line with a *Balzers Instruments Thermostar* mass spectrometer (MS), which recorded the signals at 44, 28, 18 and 14 atomic numbers, corresponding to CO_2, CO, H_2O and N_2, respectively. However, the

CO_2 signal was used to determine the coke content of the deactivated catalysts, as the H_2O formed during the combustion cannot be distinguished from CO, which in turn is immediately oxidized to CO_2 activated by the metallic function of the catalyst. The procedure followed for coke determination is as follows: stripping with N_2 (50 mL min^{-1}) at 100 °C to remove the impurities, and heating with air (50 mL min^{-1}) to 800 °C following a 5 °C min^{-1} heating rate, with that temperature being kept for 30 min for full coke combustion.

In addition, transmission electron microscopy (TEM) images (*Philips CM200*) were used to study the nature and location of the coke deposited on the catalyst.

Experimental equipment

Figure 1 shows a general scheme of a continuous steam reforming bench scale unit made up of a conical spouted bed reactor (CSBR) for the pyrolysis step and a fluidized bed reactor (FBR) for the in-line reforming of the pyrolysis volatiles. The CSBR was especially designed for the pyrolysis step [60], as it allows high heat and mass transfer rates and short residence times of the volatile products. The suitable reactor design also avoids operational problems related to the sticky nature and low thermal conductivity of molten polymers. The CSBR is located inside a radiant oven (1250 W), which allowed operating up to 900 °C. A gas preheating section filled with an inert ceramic material is placed in the lower section of the CSBR to improve heat transfer and ensure narrow temperature distribution inside the reactor. The upper section of the CSBR is the reaction zone and was designed with specific dimensions to provide a suitable spouting regime under a wide range of operating conditions. The main dimensions of the CSBR are as follow: diameter of the cylindrical section, 60.3 mm; height of the conical section, 7.3 mm; diameter of the bed bottom, 12.5 mm; angle of the conical section, 30 °; and diameter of the gas inlet, 7.6 mm. Two K-type thermocouples were located inside the reactor, one in the bed annulus and the other one close to the wall to control the reactor temperature.

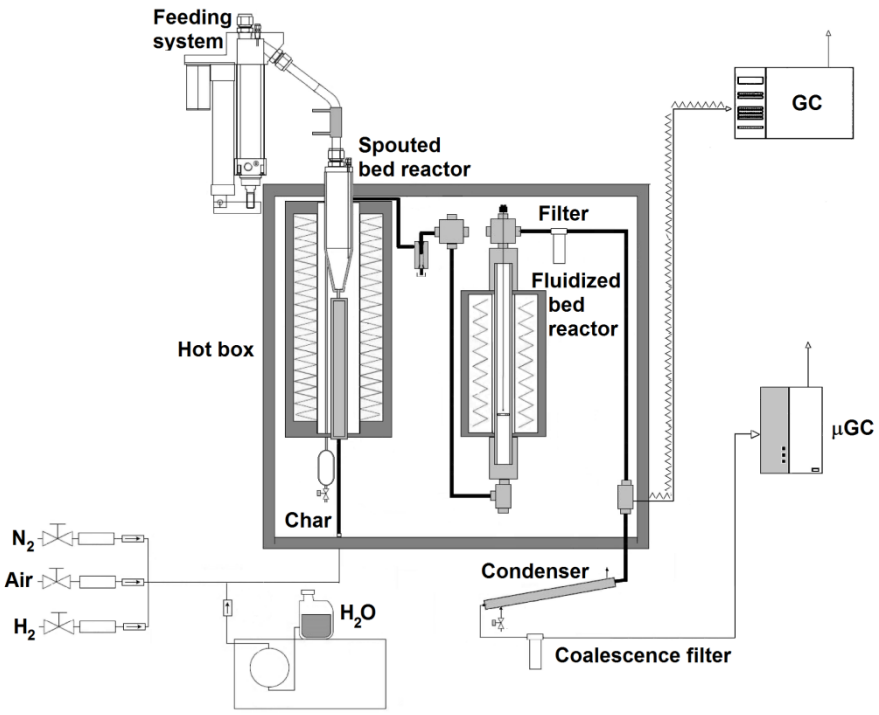

Figure 1. Representation of the continuous bench scale pyrolysis-reforming plant.

Given the operation limitations in a fixed bed reactor due to problems related to severe carbon deposition, a FBR was used for the steam reforming of the nascent volatiles formed in the CSBR. As proven in a previous study, the hydrodynamic regime of catalyst and inert particles in the FBR is close to perfect mixing [61]. The total height and internal diameter of the FBR reactor are 440 and 38.1 mm, respectively. Furthermore, the feeding system designed on purpose for the pyrolysis-reforming process allowed suitable operation in continuous regime. The feeder consists of a cylindrical vessel equipped with a vertical shaft connected to a piston placed below the plastic bed. The plastic raw material was fed into the reactor by raising the piston while an electrical motor vibrated the whole system. In addition, tap water was used to cool the pipe that conveyed the plastic from the feeder to the reactor, thus avoiding plastic melting and tube clogging. In addition, a very small nitrogen flow rate was introduced into the feeding system to avoid pyrolysis products entering the feeding system.

At the outlet of the forced convection oven, a double-shell tube condenser cooled with tap water was located to condense the non-reacted steam and pyrolysis products. Finally, a coalescence filter ensured total retention of liquid hydrocarbons prior to gas micro-chromatograph analysis.

Experimental procedure

Previous studies conducted by the research group showed that a temperature of 500 °C is the most suitable for the pyrolysis step in the set-up described above [60]. Polypropylene (PP) was continuously fed into the pyrolysis and in-line reforming unit with a rate of 0.75 g min^{-1}. Furthermore, the particle size of the sand and the steam flow rate are conditioned by the hydrodynamic requirements of the CSBR. It is to note that steam was the only fluidizing agent in both reactors, i.e., no inert gas was used. A water flow rate of 3 mL min^{-1} was established as suitable based on these requirements, which corresponds to a steam flow rate of 3.73 NL min^{-1}. In addition, 30 g of sand with a size in the 0.30–0.35 mm range were used to achieve efficient gas-solid contact and high turbulence in the bed. Concerning the reforming reactor, a temperature of 700 °C was chosen as most suitable and, based on hydrodynamic runs were carried out in the FBR with a bed amount of 25 g, particle sizes in the 0.30-0.35 mm and 0.40–0.80 mm ranges were selected as most suitable for the sand and catalyst, respectively. The experiments performed with the prepared catalysts were carried out using two different space times (4.1 and 16.7 g_{cat} min $g_{plastic}^{-1}$) and a steam/PP ratio (S/P) of 4.

Product analysis

The final products were analyzed in-line using a gas micro-chromatograph for permanent gases (micro GC Varian 4900) and gas chromatograph for the volatile ones (GC Varian 3900). The gas chromatograph was equipped with a flame ionization detector (FID) and a HP-Pona column. The gas micro-chromatograph had four channels with four analytical modules, as well as injector, columns and detector. To quantify the concentration of non-condensable gases, this gas micro-chromatograph was used with the sampling point being placed downstream the devices for condensing and filtering the gas. Samples were injected into the GC instrument by means of

a line thermostated at 280 °C, with reproducibility being ensured by several replicates under the same conditions.

Reaction indices

For the assessment of process results, individual product yields and conversion have been considered. Polypropylene conversion has been defined similarly as carbon (C) conversion efficiency in gasification processes; that is, the ratio between the moles of carbon recovered in the gaseous product and those fed in the polypropylene:

$$X_{PP} = \frac{C_{Gas}}{C_{PP}} \times 100 \quad (1)$$

The yield of C containing individual compounds is defined by mass unit of PP in the feed:

$$Y_i = \frac{F_i}{F_{PP}} \times 100 \quad (2)$$

where F_{PP} and F_i are the molar flow rates of PP and product i, respectively, both expressed in C equivalent moles.

In addition, hydrogen production has been defined by mass unit of the polypropylene in the feed:

$$P_{H2} = \frac{m_{H2}}{m_{PP}} \times 100 \quad (3)$$

where m_{H2} is the mass flow rate of the H_2 produced and m_{PP} is the mass flow rate of the polypropylene fed into the CSBR, respectively. The following stoichiometry equation was considered:

$$C_nH_m + 2nH_2O \rightarrow nCO_2 + (2n + m/2)H_2 \quad (4)$$

Results

Fresh catalyst characterization

The fresh catalysts were characterized by nitrogen adsorption/desorption, X-ray fluorescence spectroscopy (XRF), temperature programmed reduction (TPR) and X-ray diffraction (XRD). Moreover, spent catalysts were also analyzed using temperature programmed oxidation (TPO) and transmission electron microscopy (TEM) techniques. Table 1 shows the characteristics of the prepared catalysts, such as BET specific surface area, pore volume, average pore size and Ni content. The BET theory has been used to determine the catalysts surface area using the nitrogen penetration into the internal surfaces of the catalysts. Accordingly, certain points should be considered to explain the values obtained for the surface area of the catalysts. On the one hand, CeO_2 and La_2O_3 promoters significantly contribute to the weight of the prepared catalysts, and therefore they reduce the surface area. On the other hand, as these promoter particles are deposited on the catalyst pores, they hinder nitrogen access to the pores, and therefore decrease the surface area.

The results show that the surface area of the catalysts was reduced after CeO_2 and La_2O_3 impregnation, with this effect being more marked for the latter promoter. Thus, the surface area of 76 m^2g^{-1} obtained for Ni/ Al_2O_3 catalyst was reduce to 66 and 52 m^2g^{-1} in the case of Ni/CeO_2-Al_2O_3 and Ni/La_2O_3-Al_2O_3, respectively. The smaller size of CeO_2 particles compared to La_2O_3 avoided fine pore blockage when the promoters were deposited on the porous surface of the support. Therefore, the average pore size increased from 182 to 214 Å for Ni/La_2O_3-Al_2O_3, whereas the size remained almost constant for Ni/CeO_2-Al_2O_3. A similar trend was reported in various papers [62]. In addition, the amount of promoter deposited on the catalyst surface is another factor affecting the basic features of the catalysts [63, 64].

Table 1. Physical properties and those of the metal in the catalysts used.

Catalyst	**Metal content**	$\mathbf{S_{BET}}$	$\mathbf{V_{pore}}$	$\mathbf{d_{pore}}$	$\mathbf{d_{Ni\ XRD}}$ [a]	**Ni dispersion**[b]	**Total acidity**
	wt%	$m^2\,g^{-1}$	$cm^3\,g^{-1}$	Å	nm	%	$\mu mol_{NH3}\,g^{-1}$

Ni/Al_2O_3	9.8	76	0.39	182	10	9.7	265
Ni/CeO_2-Al_2O_3	8.2	66	0.36	181	18	5.4	139
Ni/La_2O_3-Al_2O_3	8.1	52	0.39	214	20	4.9	83

[a] Calculated from the full width at half the maximum of the Ni (2 0 0) diffraction peak at 2θ = 52 ° in the XRD using the Scherrer equation.

[b] Dispersion calculated by (97.1 nm)/(Particle size of Ni (nm)).

The results of the XRF device show that the nickel content in the Ni/Al_2O_3 catalyst (9.8 wt%) is that corresponding to the nominal amount (10 wt%), which is evidence that the preparation method was appropriate and almost all Ni particles were deposited on the catalyst. In the two promoted catalysts, however, nickel content is slightly lower, between 8.1 and 8.2 wt%. The lower surface area, pore blockage and lower access to the catalyst internal pores, as well as the steric hindrance of the promoters, especially La_2O_3, are the main factors reducing Ni dispersion in the promoted catalysts. Accordingly, the value of 9.7 % reached in the Ni/Al_2O_3 catalyst decreased to 5.4 and 4.9 % for Ni/CeO_2-Al_2O_3 and Ni/La_2O_3-Al_2O_3 catalysts, respectively. The total catalyst acidity determined by NH_3 adsorption-desorption is also shown in Table 1. As observed, Ni/Al_2O_3 catalyst revealed the highest acidity (265 μmol g^{-1}) compared to the promoted catalysts (139 and 83 μmol g^{-1} for Ni/CeO_2-Al_2O_3 and Ni/La_2O_3-Al_2O_3 catalysts, respectively). These results are evidence of the role of the basic promoter to reduce the acid sites of the Al_2O_3 support, which may contribute to hindering the secondary reactions leading to coke deposition. [65-67]

The TPR profile of the prepared catalysts is shown in Figure 2. As observed, there is a weak peak at about 450 ºC in the three catalysts, which is related to the reduction of NiO weakly interacting with the support [68, 69]. In addition, the profile for Ni/Al_2O_3 catalyst shows two very strong peaks at temperatures close to 600 and above 700 ºC. The peak close to 600 ºC is associated with the reduction of dispersed NiO species, which interact strongly with Al_2O_3 [70].

The peak observed above 700 °C is due to the Ni particles that have migrated on the Al_2O_3 surface to form $NiAl_2O_4$, which is resistant to reduction and stable even at 900 °C [71]. The Ni/CeO_2-Al_2O_3 catalyst, similarly to Ni/Al_2O_3, shows two strong reduction peaks, which shift to lower temperatures (~ 550 and 710 °C) when CeO_2 is used as promoter. This peak shifting is evidence that CeO_2 promoter weakens the interaction of NiO with Al_2O_3 [62]. At higher temperature (> 800 °C), a small reduction peak is observed, which is associated with the reduction of bulk ceria crystallites related to $CeAlO_3$ formation [49]. The addition of La_2O_3 promoter to the Ni/Al_2O_3 catalyst increases the reduction capacity of NiO species strongly interacting with the support (peak at around 700 °C). In the Ni/La_2O_3-Al_2O_3 catalyst, a decrease in the $NiAl_2O_4$ phase is also observed, thereby improving the reducibility of the Ni/Al_2O_3 catalyst [57].

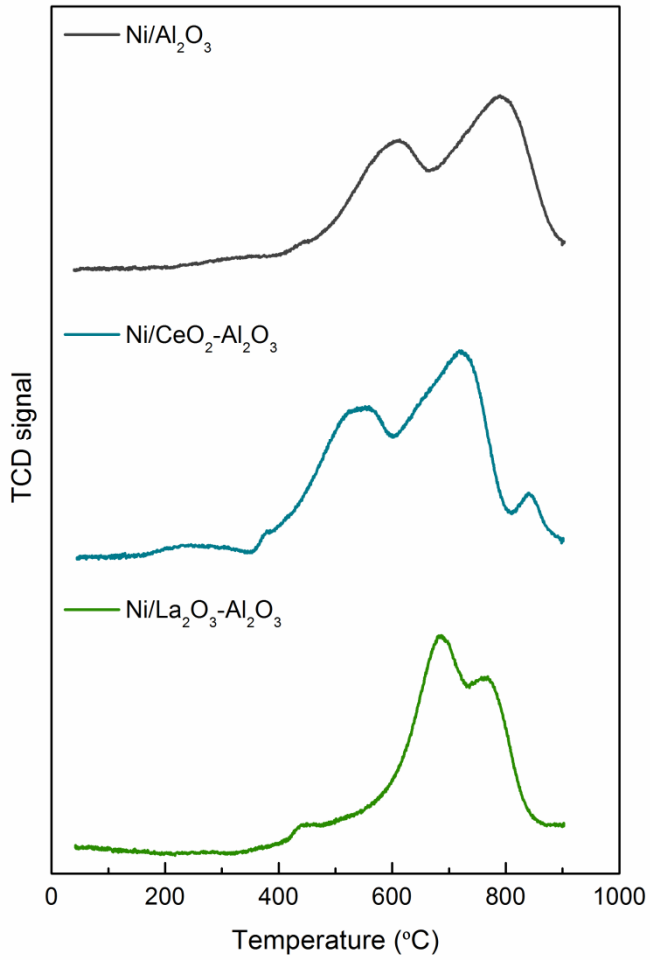

Figure 2. TPR profiles of Ni/Al_2O_3, Ni/CeO_2-Al_2O_3 and Ni/La_2O_3-Al_2O_3 catalysts.

Figure 3 shows the XRD patterns of the three prepared catalysts. Groups with strong diffraction lines, such as those corresponding to Ni phase, Al_2O_3, CeO_2 and $CeAlO_3$, are clearly detectable, while many groups are not detectable. At 2θ = 44 °, 52 ° and 76 °, diffraction lines related to crystalline Ni phases are observed in the catalyst samples, which correspond to (1 1 1), (2 0 0) and (2 2 0) planes, respectively [72], whereas NiO is fully reduced and not detected. In addition, Al_2O_3 showed the typical detectable diffraction peaks in the three catalysts, apart from those corresponding to the Ni phase. However, XRD cannot detect the $NiAl_2O_4$ spinel because the related phase diffraction lines (2θ = 29 °, 45 ° and 60 ° [71]) overlap those of Al_2O_3 phase [48, 73]. Likewise, regarding these catalysts, the $NiAl_2O_4$ spinel phase is not detectable using this

technique. XRD can be used to identify different groups, but they overlap in many cases and the weaker diffraction lines cannot be detected. Concerning Ni/La_2O_3-Al_2O_3, the peaks corresponding to Ni and Al_2O_3 species severely overlap due to the low crystallinity of La_2O_3, and therefore a weak response to X ray (weak and broad peaks) is obtained, i.e., La species are not detectable using XRD technique [66, 74]. Yamamoto et al. [75] showed that La groups are not detectable even for loadings above 25 wt% La_2O_3, which is evidence that La_2O_3 levels do not play a significant role in identification. Concerning Ni/CeO_2-Al_2O_3 catalyst, the spinel phase diffraction lines are detected for $CeAlO_3$ at 2θ = 23 °, 44 °, 47 ° and 60 °, and the diffraction lines of CeO_2 are identified at 2θ = 28 °, 33 °, 47 ° and 56 °. Concerning the prepared catalysts, the Ni crystal size was calculated using XRD patterns and applying the Debye-Scherrer equation to 2θ = 52 ° diffraction bands. Various studies have shown that, due to the decrease in the catalyst surface area, active phase dispersion and Ni deposition on the catalyst surface decrease and the Ni crystal size increases clearly [50, 57].

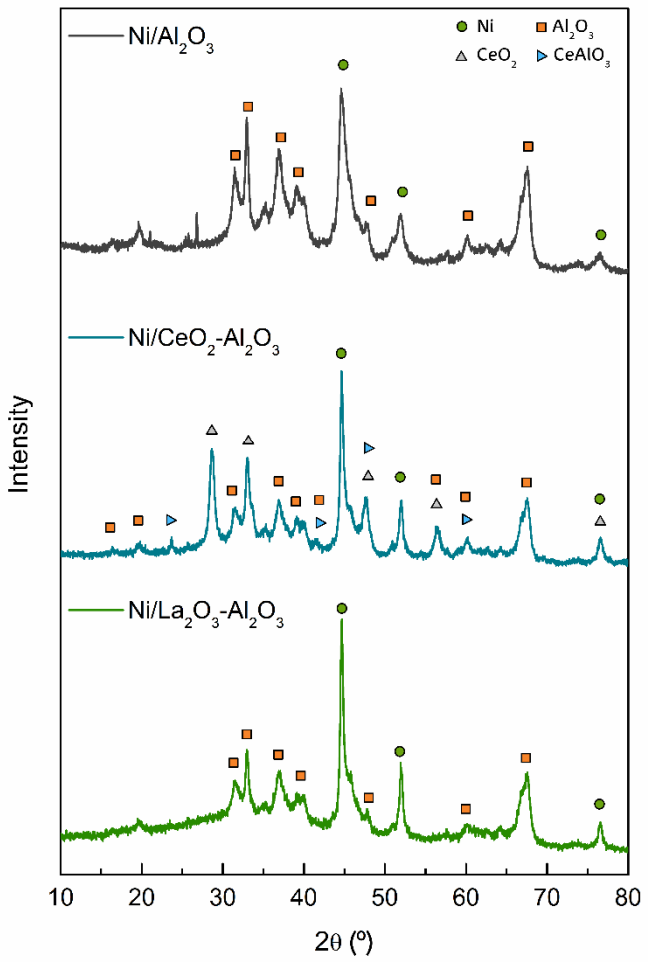

Figure 3. XRD patterns of the reduced catalysts.

Pyrolysis step

In order to evaluate the performance of the different reforming catalysts proposed, a good knowledge of the composition of the product stream entering the reforming step is required. Accordingly, the pyrolysis volatiles obtained in PP degradation at 500 ºC were analyzed. It should be noted that the pyrolysis process was carried out under steam atmosphere, which is the fluidizing agent in the pyrolysis step and reacts with PP pyrolysis products in the subsequent reforming step. Furthermore, under the mild pyrolysis conditions used in this study, it has a negligible impact on the pyrolysis product distributions, with the results obtained being comparable to those obtained using nitrogen as fluidizing agent [16, 28].

The CSBR allows for operating under fast pyrolysis conditions, with high heating rates and short residence times of volatile stream. These conditions attenuate secondary reactions, and therefore primary pyrolysis products, such as waxes, were the prevailing ones. Waxes are made up of heavy hydrocarbons of linear or branched nature. Their yield was of 74.8 %, with 32.5 % corresponding to light ones (C_{21}-C_{40}) and the remaining 42.3 % to the heavy fraction (C_{41}^{+}). Moreover, the yield of liquid products was of 23.9 %. This oil was mainly in the diesel range (C_{12}-C_{20}), 19.2 %, with the yield of the gasoline fraction (C_5-C_{11}) being of 4.7 %. Finally, the yield of gaseous products was low, 1.3 %. It is to note that PP was fully converted into volatile products and no solid residue was formed in the PP pyrolysis at 500 ºC. These results are consistent with the results reported in the pyrolysis of polyolefins in different reactors under fast pyrolysis conditions [76-78].

Evaluation of catalyst performance

Three homemade catalysts (Ni/Al_2O_3, Ni/CeO_2-Al_2O_3 and Ni/La_2O_3-Al_2O_3) operated with two space times (4.1 and 16.7 g_{cat} min $g_{plastic}^{-1}$) have been studied by monitoring the conversion and product yields in the reforming of PP pyrolysis volatiles. As mentioned in the previous sections, a conical spouted bed reactor (CSBR) was used to pyrolyze polypropylene and a fluidized bed reactor (FBR) to reform in-line the hydrocarbon volatiles from the pyrolysis step. It is to note that the following main reactions take place in the reforming reactor:

Steam reforming of hydrocarbons: $C_nH_m + nH_2O \rightarrow nCO + (n + m/2)H_2$ (5)

Water gas shift (WGS): $CO + H_2O \Leftrightarrow CO_2 + H_2$ (6)

Fig. 4 shows the evolution of conversion (%) and hydrogen production (%) for the three homemade catalysts operated with two space times. As observed, when the higher space time (16.7 g_{cat} min $g_{plastic}^{-1}$) is used, the three catalysts performed better in terms of conversion and hydrogen production. Thus, almost full conversion was attained and hydrogen production was of about 34 %, while the lower space time (4.1 g_{cat} min $g_{plastic}^{-1}$) led to a conversion in the 74.7 to

80.7 % range and hydrogen production between 20.7 and 24.9 %. It should be noted that the non-converted fraction corresponds to the liquid hydrocarbons (C_{5+} fraction), according to the definition of conversion considered in this study (Eq. 1).As observed, the performance of the catalysts used at both space times is as follows: Ni/La_2O_3-Al_2O_3 > Ni/Al_2O_3 > Ni/CeO_2-Al_2O_3. It should be noted that the in-line pyrolysis-reforming process showed a remarkable potential for hydrogen production with all the catalysts tested. Moreover, full conversion of pyrolysis products with a space time of 16.7 g_{cat} min $g_{plastic}^{-1}$ allows for the production of a tar free syngas. The lowest conversion and H_2 production were obtained when the Ni/CeO_2-Al_2O_3 catalyst was used, which is even lower than that corresponding to the Ni/Al_2O_3 catalyst. This is partially explained by the lower Ni content in the former. Although CeO_2 addition to the Ni/Al_2O_3 catalyst improves the performance in the biomass pyrolysis-reforming process [50], this effect is negligible when PP is valorized due to the different composition of the volatiles fed into the reforming step. In spite of the lower Ni content of Ni/La_2O_3-Al_2O_3 catalyst compared to Ni/Al_2O_3, La_2O_3 addition has a positive effect on conversion and H_2 production. Czernik and French [79] reported similar hydrogen production values (34 %) in the in-line reforming of PP pyrolysis volatiles over a Ni commercial catalyst in a continuous reaction unit made up of two fluidized bed reactors. The use of a Ru/Al_2O_3 catalyst in a reaction unit based on two continuous fixed beds for the pyrolysis and in-line steam reforming of PP led to a maximum hydrogen production of 36 % [25]. Lower hydrogen productions (below 26.6 %) were reported by Wu and Williams [24] in a batch unit with two fixed bed reactors, in which they used $Ni/MgO/Al_2O_3$ catalysts. Yao et al. [34] analyzed the performance of Ni/Al_2O_3 catalysts prepared following different methodologies in the PP pyrolysis-reforming in a batch unit including two fixed bed reactors, and they obtained hydrogen productions between 9.2 and 13.4 %. Recently, Yao et al. [19] reported hydrogen productions in the 11 to 13 % range using Ni based catalysts supported on different zeolites. It should also be noted that polymers with linear structure and high hydrogen content (high H/C ratio), such as polyethylene and polypropylene, have a lower tendency to form cyclic and aromatic products during pyrolysis, and therefore perform better in pyrolysis-reforming compared to other polymers containing aromatic structures and oxygen, such as PET

[18, 28], polyurethanes [35] and polystyrene [13, 24, 26, 28, 29]. Thus, Barbarias et al. [26] reported a H_2 production of 29.1 % in the pyrolysis-reforming of PS using a Ni/Al_2O_3 commercial catalyst in the same experimental unit as in this study. In the same line, Namioka et al. [13] obtained a higher hydrogen production when PP was in the feed (36%) than when PS was the raw material (33 %). Zhou et al. [17] reported the maximum H_2 production in the PS pyrolysis reforming over a Ni-Fe/ZrO_2 was at 500 ºC in a reaction unit made up of two fixed bed reactors. Saad and Williams [27] performed a detailed study, in which they compared the dry reforming of different plastics over a Ni-Co/Al_2O_3 catalyst, and H_2 production decreased from 15 % when the feed was PE to 7.6 and 2.5 % when the feeds were PS and PET, respectively. In the same line, the hydrogen productions reported in biomass pyrolysis-reforming are also markedly lower, i.e., 11 % under optimum process conditions and highly active catalysts [14, 80-82].

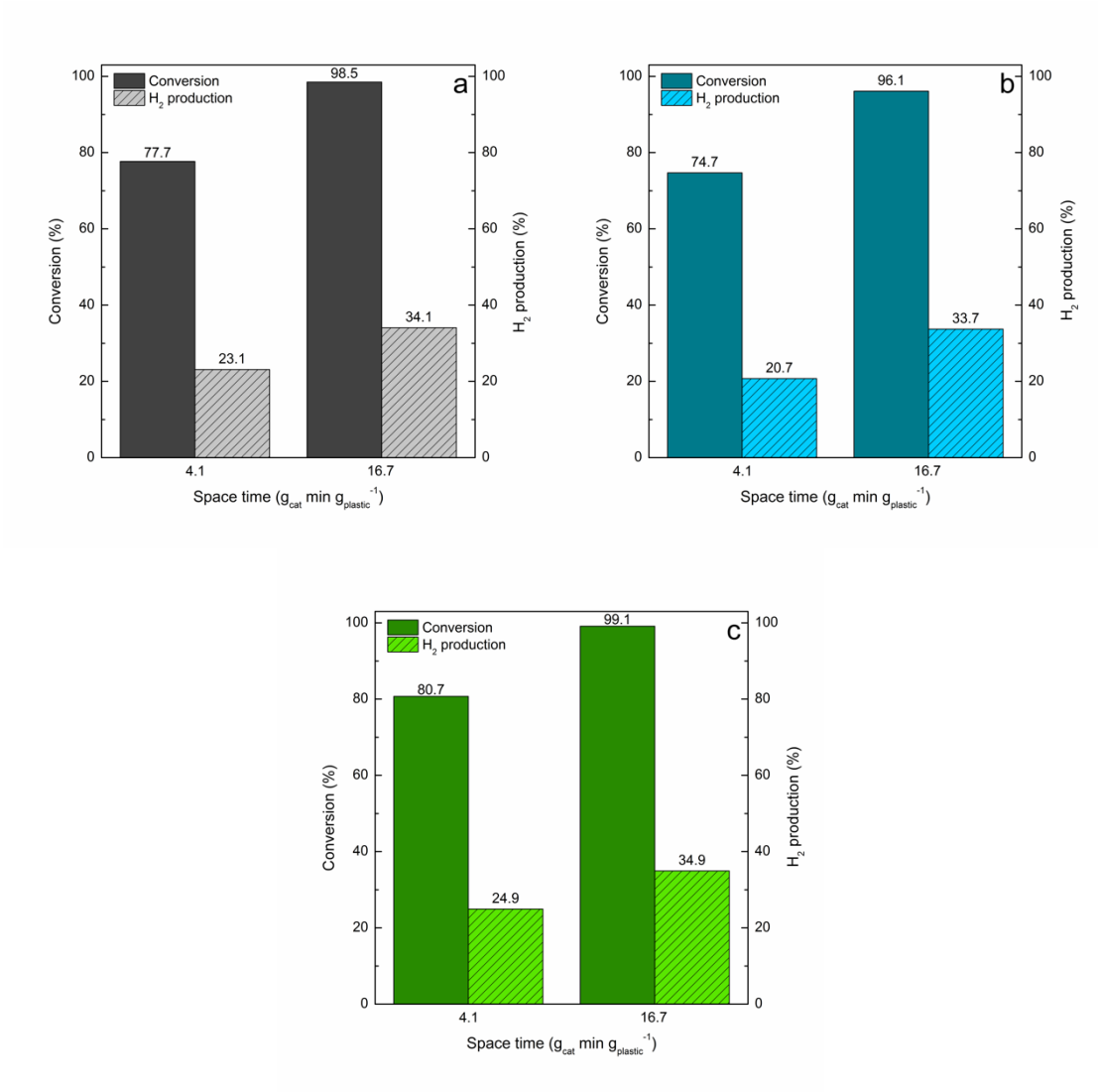

Figure 4. Conversion and hydrogen productions obtained in the reforming of PP pyrolysis volatiles with space times of 4.1 and 16.7 g_{cat} min $g_{plastic}^{-1}$ over Ni/Al_2O_3 (a), Ni/CeO_2-Al_2O_3 (b) and Ni/La_2O_3-Al_2O_3 (c) catalysts.

Figure 5 shows the yields of the products obtained with the three prepared catalysts operated with the two space times. The results show that space time has a great impact on product yields. In fact, a space time of 4.1 g_{cat} min $g_{plastic}^{-1}$ leads to a significant fraction of non-converted PP pyrolysis products (C_5+). However, these experiments performed under kinetic control conditions allow determining the higher activity of Ni/La_2O_3-Al_2O_3 catalyst for steam reforming (Eq. 5) and, especially, for promoting the WGS (Eq. 6) reaction, which is evidenced by the

higher H_2 and CO_2 yields in relation to those obtained with the conventional Ni/Al_2O_3 and CeO_2 promoted catalyst.

Operating with a space time of 16.7 g_{cat} min $g_{plastic}^{-1}$, almost complete conversion was reached and the three catalysts performed well compared to the lower space time. In general, the Ni/La_2O_3-Al_2O_3 catalyst with the space time of 16.7 g_{cat} min $g_{plastic}^{-1}$ produced high yields of H_2, CO, and CO_2 and the yield of residual hydrocarbons (including gaseous and liquid ones) is almost negligible (~1.5%) at zero time on stream. However, the Ni/CeO_2-Al_2O_3 and Ni/Al_2O_3 catalysts showed a poorer reforming performance leading to a remarkable yield of residual hydrocarbons, 7.5 and 2.9 %, respectively. In the same line, the use of Ni/La_2O_3-Al_2O_3 catalyst also favored the WGS reaction by shifting it towards the formation of H_2 and CO_2.

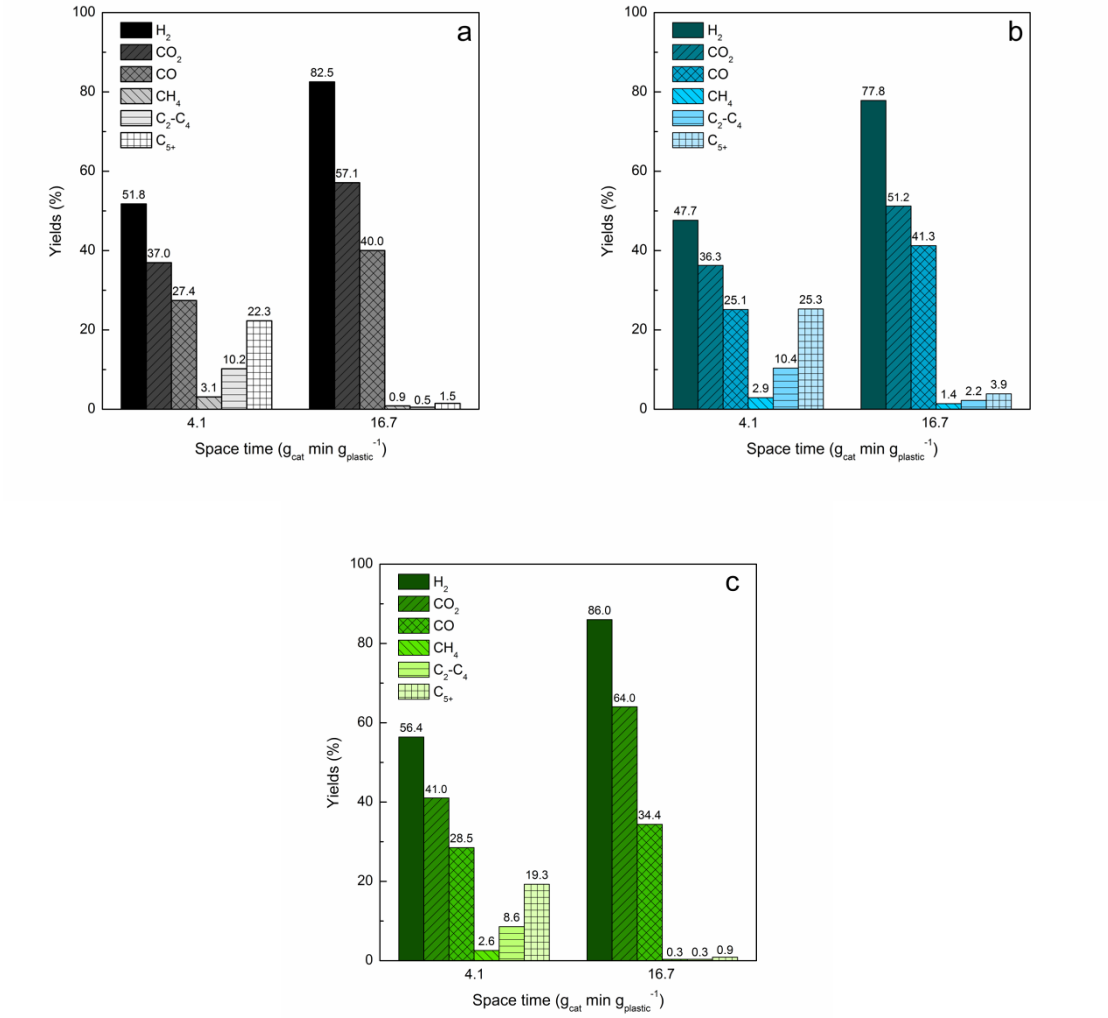

Figure 5. Individual product yields obtained in the reforming of PP pyrolysis volatiles with the space times of 4.1 and 16.7 g_{cat} min $g_{plastic}^{-1}$ over Ni/Al_2O_3 (a), Ni/CeO_2-Al_2O_3 (b) and Ni/La_2O_3-Al_2O_3 (c) catalysts.

The results at zero time on stream clearly show that the Ni/La_2O_3-Al_2O_3 catalyst is the one of best performance. However, a suitable catalyst for this process should also consider stability. Thus, Figure 6 shows the evolution with time on stream of conversion and hydrogen production for the three prepared catalysts used with the space time of 16.7 g_{cat} min $g_{plastic}^{-1}$. The results show that the activity of the three catalysts decreased almost linearly, which is evidence of a progressive reduction of conversion and hydrogen production with time. As can be seen, Ni/Al_2O_3 and Ni/CeO_2-Al_2O_3 catalysts show more a pronounced activity decline over time, while the Ni/La_2O_3-Al_2O_3 catalyst performs better concerning conversion and hydrogen production throughout time. Thus, conversion decreases from full one at the beginning to 91 % after 200 min continuous operation with Ni/La_2O_3-Al_2O_3 catalyst. It is to note that the use of La_2O_3 as promoter reduces alumina acidity and inhibits coke formation [66]. Moreover, it also promotes water adsorption and dissociation and gasifies the deposited coke, preventing catalyst deactivation [83, 84]. The Ni/Al_2O_3 catalyst showed a faster deactivation rate than the Ni/La_2O_3-Al_2O_3 catalyst, thus conversion decreasing to 86 % after 200 min operation. Although the conversion attained with the Ni/CeO_2-Al_2O_3 catalyst after 200 min was of 84%, the lower initial activity should be also considered for the evaluation of its stability. In fact, the conversion drop throughout the reaction process is lower than in the case of the non-promoted Ni/Al_2O_3 catalyst. Interestingly, the deactivation rates observed in the reforming of PP pyrolysis products were remarkably lower than those observed in biomass pyrolysis-reforming with the same catalysts and under similar operating conditions [50, 57].

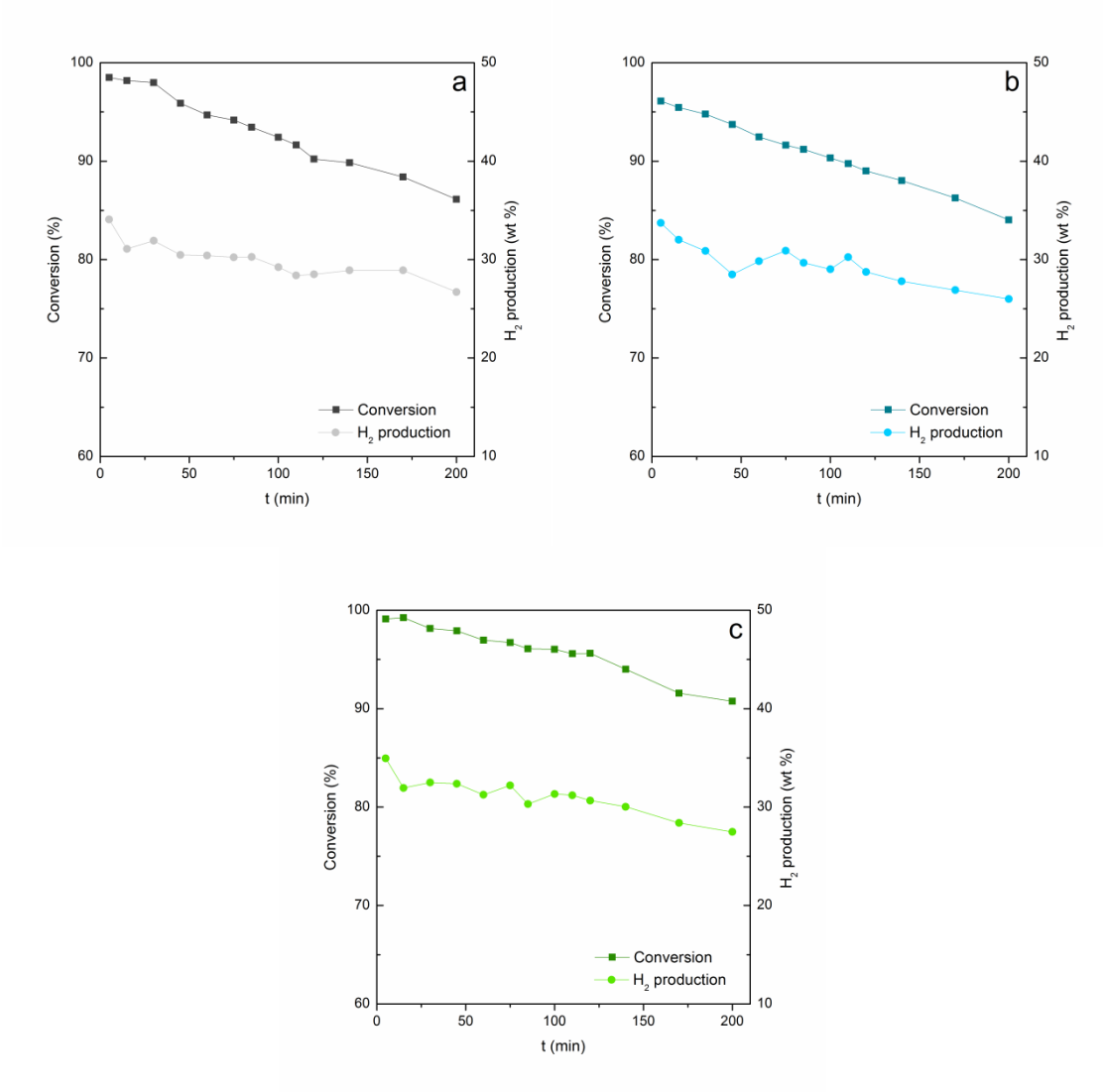

Figure 6. Evolution with time on stream of conversion and hydrogen production in the reforming of PP pyrolysis volatiles with a space time 16.7 g_{cat} min $g_{plastic}^{-1}$ over Ni/Al_2O_3 (a), Ni/CeO_2-Al_2O_3 (b) and Ni/La_2O_3-Al_2O_3 (c) catalysts.

Figure 7 shows the yields of the products obtained throughout time in the reforming on the three catalysts with the space time of 16.7 g_{cat} min $g_{plastic}^{-1}$. The results show that the yield of hydrogen decreases steadily over time on stream from 84 to 62 %, from 78 to 62 % and from 86 to 66 % when Ni/Al_2O_3, Ni/CeO_2-Al_2O_3 and Ni/La_2O_3-Al_2O_3 catalysts were used, respectively, with this reduction being higher in the non-promoted catalyst. Moreover, as the reaction time increased and the catalytic activity decreased, the CO_2 yield decreased and CO yield increased to certain extent (especially on Ni/La_2O_3-Al_2O_3 and Ni/Al_2O_3). Therefore, the reduction of catalyst activity

for steam reforming (Eq. 5) and the WGS (Eq. 6) reaction explain the evolutions of H_2, CO and CO_2. In addition, the results show that the yields of non-converted C_5^+ and lighter hydrocarbons progressively increase with the advance of time on stream and so decay of catalytic activity. In view of the results, the Ni/La_2O_3-Al_2O_3 catalyst showed higher efficiency and stability than Ni/Al_2O_3 and Ni/CeO_2-Al_2O_3.

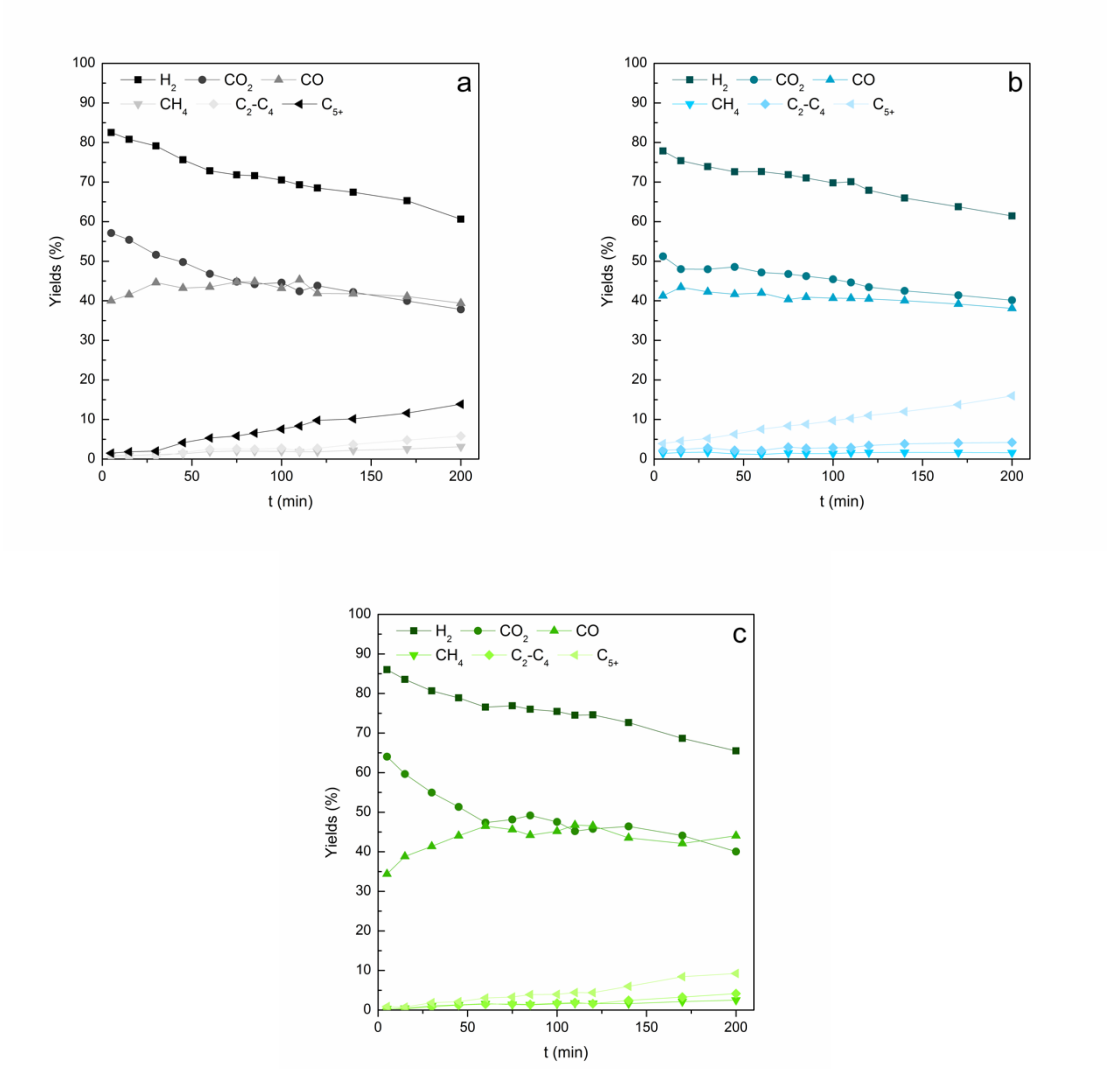

Figure 7. Evolution with time on stream of individual product yields in the reforming of PP pyrolysis volatiles with a space time 16.7 g_{cat} min $g_{plastic}^{-1}$ over Ni/Al_2O_3 (a), Ni/CeO_2-Al_2O_3 (b) and Ni/La_2O_3-Al_2O_3 (c) catalysts.

Catalyst deactivation

The suitable performance of a reforming catalyst depends on many parameters such as conversion, hydrogen production, and catalyst activity and stability. Another parameter affecting catalyst performance is the composition of the input feed. Feeds like polyethylene and polypropylene (with high hydrogen content and low tendency to Diels-Alder reactions and coke production) lead to an almost linear inactivation [28]. However, biomass, PS and PET pyrolysis volatiles contain high amounts of aromatic and oxygenated compound, and they therefore lead to coke formation [28]. Accordingly, the decrease in catalytic activity usually follows an exponential trend [26, 58]. Moreover, the performance of tje reforming catalyst can also be conditioned by the stability of the metallic phase [85, 86]. Therefore, the causes of catalyst deactivation are analyzed in this section by considering coke deposition and Ni sintering as the more plausible causes according to previous results [50, 57].

Figure 8 shows the XRD patterns of the spent catalysts used for 200 min stream time. It should be noted that there are no significant differences compared to the fresh catalysts (Figure 3). In addition, the Ni crystalline phases are observed at 2θ = 44 °, 52 ° and 76 ° for the studied catalysts, while the diffraction lines of NiO are not identified, which is evidence that the catalysts are not deactivated due to active phase oxidation. The spent Ni/CeO_2-Al_2O_3 catalyst shows no diffraction line at 2θ = 34 °, while the deactivated Ni/CeO_2-Al_2O_3 catalyst used in biomass reforming recorded a diffraction line corresponding to $CeAlO_3$ spinel phase [50]. The XRD results also show that the nature of Ni/La_2O_3-Al_2O_3 catalyst had not changed. In addition, by applying the Scherrer equation for the diffraction peak at 2θ = 52 °, the Ni crystallite size has been calculated to ascertain catalyst irreversible deactivation by Ni sintering for the fresh and spent catalysts (Table 2). Compared to the fresh catalysts, the Ni crystallite size does not increase considerably, and therefore the deactivation observed for these catalysts is not due to Ni sintering. However, the Ni crystallite size of the spent Ni/CeO_2-Al_2O_3 catalyst has hardly changed (~ 18-19 nm).

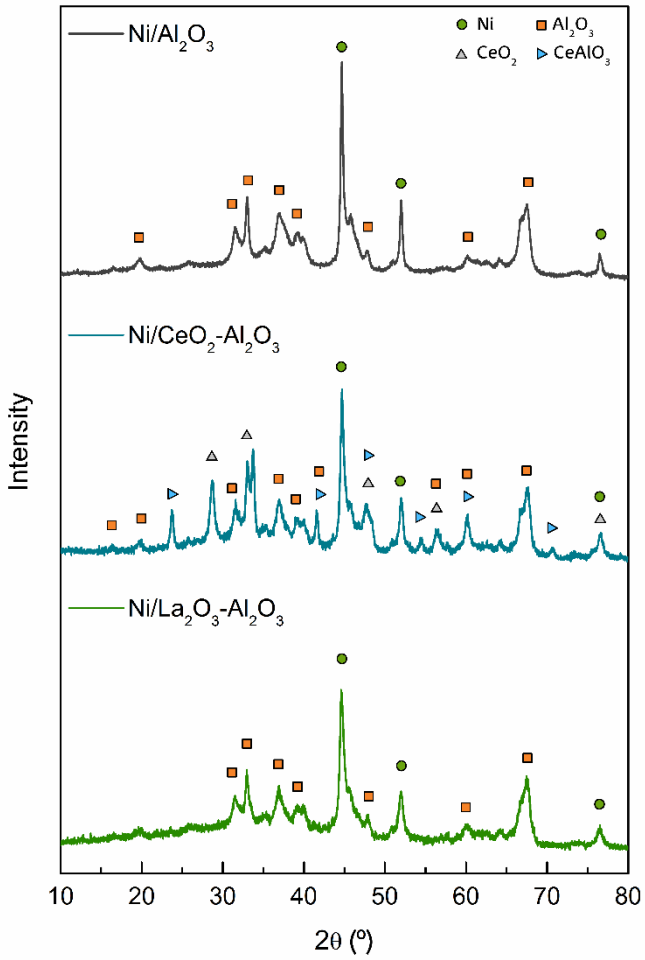

Figure 8. X-ray diffraction (XRD) profiles of the spent Ni/Al_2O_3, Ni/CeO_2-Al_2O_3 and Ni/La_2O_3-Al_2O_3 catalysts.

The nature, location and amount of the deposited coke were analyzed based on the temperature programmed oxidation (TPO). The results of coke deposited on the used catalysts have been summarized in Table 2 and their TPO profiles have been plotted in Figure 9. The results show that the used Ni/La_2O_3-Al_2O_3 catalyst led to a lower amount of coke deposited (2.24 wt%) compared to Ni/CeO_2-Al_2O_3 (3.46 wt%) and Ni/Al_2O_3 (3.75 wt%) catalysts. The average coke deposition per plastic mass unit fed into the process (r_c) is a practical parameter for comparing the amount of coke deposited in different catalysts, and is defined as follows [50]:

$$r_{coke}=\frac{W_{coke}/t}{W_{cat}\, m_{PP}} \quad (7)$$

where W_{coke} and W_{cat} are coke and catalyst masses, respectively, m_{PP} the feed rate and t the time on stream.

Table 2 shows the average coke deposition rate (r_c) for the reforming catalysts, which is directly related to the amount of coke produced for the continuous operation with the three catalysts. As can be seen, the Ni/La_2O_3-Al_2O_3 catalyst had a lower coke deposition rate (0.15 mg_{coke} g_{cat}^{-1} $g_{plastic}^{-1}$) compared to Ni/Al_2O_3 (0.25 mg_{coke} g_{cat}^{-1} $g_{plastic}^{-1}$) and Ni/CeO_2-Al_2O_3 (0.23 mg_{coke} g_{cat}^{-1} $g_{plastic}^{-1}$) catalysts. The results also show that the promoted catalysts led to lower coke deposition rates. Thus, the incorporation of La_2O_3 promoted steam adsorption and dissociation, which favors in situ coke gasification [83, 84]. In the same line, the redox properties of CeO_2 also contribute to coke gasification [87, 88].

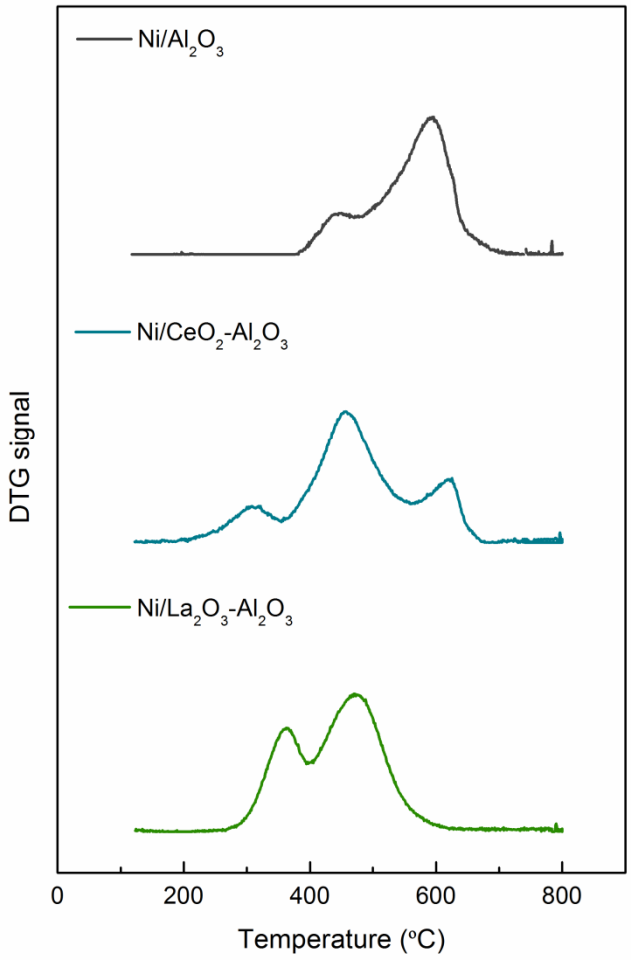

Figure 9. Temperature programmed oxidation (TPO) profiles of the catalysts deactivated for 200 min continuous operation.

Table 2. Textural and metallic properties of the deactivated Ni catalysts.

Catalyst	Metallic properties		Coke deposition		
	d_{Ni}[a] (nm)				
	Fresh	Deact.	Cc (wt%)	Time on stream (min)	r_C ($mg_{coke}\ g_{cat}^{-1}\ g_{plastic}^{-1}$)

Ni/Al_2O_3	10	13	3.75	200	0.25
Ni/La_2O_3-Al_2O_3	20	23	2.24	200	0.15
Ni/CeO_2-Al_2O_3	18	19	3.46	200	0.23

[a] Calculated from the full width at half the maximum of the Ni (2 0 0) diffraction peak at 2θ = 52 ° in the XRD using the Scherrer equation.

Figure 9 shows the TPO profiles obtained with the spent homemade catalysts. As observed, peak location and shape changed to some extent due to coke deposition. The first peak for the spent Ni/Al_2O_3 catalyst appears at around 480 ºC, corresponding to amorphous coke combustion deposited on the Ni particles. The second peak at around 600 ºC corresponds to the filamentous coke with less influence on catalyst deactivation [84]. Similarly, the two types of coke observed for used Ni/La_2O_3-Al_2O_3 catalyst burned at lower temperatures compared to Ni/Al_2O_3, which is explained by the coke hindering effect of La_2O_3 due to its water adsorption capacity during the reforming reaction [47, 89]. Previous studies dealing with biomass pyrolysis-reforming led to similar trends [57], although the ratio between the two types of cokes and their structure is totally different when plastics are valorized. Furthermore, the coke deposited on the Ni/CeO_2-Al_2O_3 catalyst burned at lower temperatures, around 300 and 480 ºC, which is related to CeO_2 promotion, enhancing water adsorption and providing redox properties to the support. Therefore, coke gasification is favoured and its evolution to a more structured coke is inhibited [90, 91]. In addition, there is a small peak at around 640 ºC, which is related to the filamentous coke. It is to note that due to the capacity of the promoted catalysts for water adsorption, which activates the gasification of the coke precursors, the amorphous carbonaceous structure is not dense enough to fully block the metallic sites, and therefore the catalysts are stable for a longer time on stream.

Figure 10 shows TEM images of the used catalysts, which may give an insight of the morphology of the deposited coke. The TEM images confirm the bigger size of Ni crystallite in

the promoted catalysts compared to the Ni/Al_2O_3 catalyst, which was also inferred based on the XRD profiles of the spent catalysts (see Table 2). Thus, the average Ni crystallite size corresponding to Ni/Al_2O_3 was 13 Å, whereas those of Ni/CeO_2-Al_2O_3 and Ni/La_2O_3-Al_2O_3 were 19 and 23 Å, respectively. As mentioned above, the filamentous nature of the coke is clearly observed. Moreover, the TEM images also show an amorphous coke without any specific morphology, whose condensation degree and location is different depending on the catalyst. These results evidence the effect feed composition has on the type of coke and its structure. When biomass pyrolysis-reforming was studied [50, 57], none of the catalysts contained filamentous coke; that is, the coke was mainly amorphous. Thus, the filamentous coke formed in the reforming of hydrocarbons produced in polyolefin pyrolysis deactivates less than the coke formed in the reforming of the oxygenate compounds derived from biomass pyrolysis [31]. Comparing the three catalysts studied, Ni/La_2O_3-Al_2O_3 has acceptable stability and undergoes the lowest coke deposition by enhancing precursor gasification [65].

The present study clearly shows a positive performance of $Ni/La_2O_3/Al_2O_3$ catalysts, as they lead to high hydrogen productions and full conversion of plastics pyrolysis volatiles at zero time on stream. In spite of the improvement in catalyst stability operating with La_2O_3 promoted catalysts, fast deactivation is still a challenge to be overcome for the full-scale development of the plastics pyrolysis reforming strategy. Given that the reforming reaction is a highly endothermic process, operation under oxidative conditions, i.e., by injecting an oxygen stream to the reforming reactor, may avoid the high heat requirement in the reforming step. Moreover, this strategy may also contribute to the in situ combustion of the coke deposited on the catalyst, and therefore attenuate catalyst deactivation [92]. Accordingly, studies dealing with the oxidative steam reforming of plastics pyrolysis volatiles will be conducted in the future, with focus being placed on the development of suitable catalysts for the operation under these conditions.

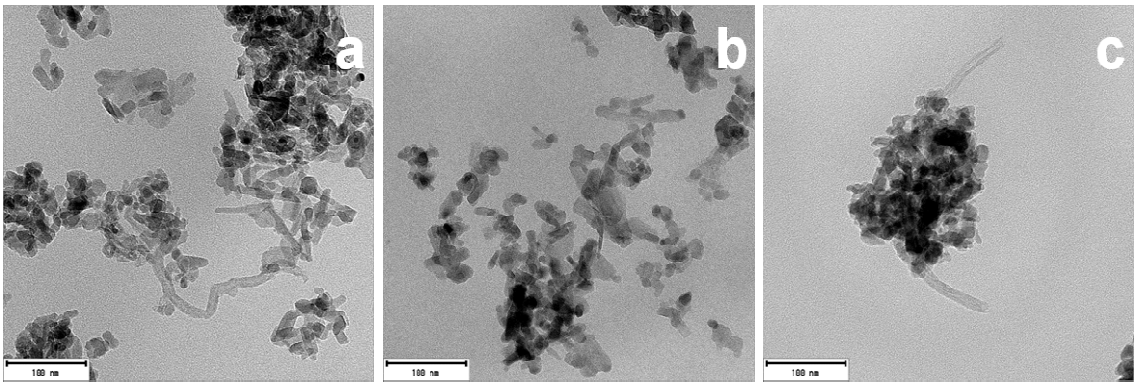

Figure 10. TEM images of deactivated Ni/Al_2O_3 (a), Ni/CeO_2-Al_2O_3 (b) and Ni/La_2O_3-Al_2O_3 (c) catalysts.

Conclusions

Ni/Al_2O_3 catalyst along with two promoted catalysts containing La_2O_3 and CeO_2 were evaluated in the steam reforming of polypropylene pyrolysis volatiles in a bench scale pyrolysis-reforming plant operating in continuous regime. The results showed that a space time of 4.1 g_{cat} min $g_{plastic}^{-1}$ is not enough, as it led to partial polypropylene conversion and rather low hydrogen production in the range of conditions studied. Nevertheless, a space time of 16.7 g_{cat} min $g_{plastic}^{-1}$ led to full conversion and high hydrogen production. Furthermore, polypropylene is a highly suitable feed for reforming, as it has a high hydrogen content and leads to a catalyst deactivation trend with almost linear trend of low slope. The used catalysts maintained their activity above 80 % for a time on stream of 200 min. The three prepared catalysts perform well in the reforming of polypropylene, although the Ni/La_2O_3-Al_2O_3 catalyst had superior performance concerning conversion, hydrogen production and coke deposition, and is therefore the most suitable one for the reforming of this feed. H_2, CO, and CO_2 were the main products of the reforming reaction together with a very small amount of hydrocarbon compounds. The TPO pattern also showed that lower temperatures are needed to burn the coke on the Ni/La_2O_3-Al_2O_3 catalyst, which is a clear advantage for catalyst regeneration.

Acknowledgments

This work was carried out with the financial support from Spain's ministries of Economy and Competitiveness (CTQ2016-75535-R (AEI/FEDER, UE), Science, Innovation and Universities (RTI2018-101678-B-I00 (MCIU/AEI/FEDER, UE)) and, Science and Innovation PID2019-107357RB-I00 (MCI/AEI/FEDER, UE)), the European Union's Horizon 2020 research and innovation programme under the Marie Skłodowska-Curie grant agreement No. 823745, and the Basque Government (IT1218-19 and KK-2020/00107).

References

1. Abbas-Abadi, M. S. The effect of process and structural parameters on the stability, thermo-mechanical and thermal degradation of polymers with hydrocarbon skeleton containing PE, PP, PS, PVC, NR, PBR and SBR. *J. Therm. Anal. Calor.* **2020,** DOI 10.1007/s10973-020-09344-0.

2. Sharma, A.; Aloysius, V.; Visvanathan, C. Recovery of plastics from dumpsites and landfills to prevent marine plastic pollution in Thailand. *Waste Dispos. Sustain. Energy* **2019,** *1,* 237-249, DOI 10.1007/s42768-019-00027-7.

3. Ragaert, K.; Delva, L.; Van Geem, K. Mechanical and chemical recycling of solid plastic waste. *Waste Manageme.* **2017,** *69,* 24-58, DOI 10.1016/j.wasman.2017.07.044.

4. Lopez, G.; Artetxe, M.; Amutio, M.; Bilbao, J.; Olazar, M. Thermochemical routes for the valorization of waste polyolefinic plastics to produce fuels and chemicals. A review. *Renew. Sustain. Energy Rev.* **2017,** *73,* 346-368, DOI 10.1016/j.rser.2017.01.142.

5. Kunwar, B.; Cheng, H. N.; Chandrashekaran, S. R.; Sharma, B. K. Plastics to fuel: a review. *Renewable Sustainable Energy Rev.* **2016,** *54,* 421-428, DOI 10.1016/j.rser.2015.10.015.

6. Nallar, M.; Wong, H. Enhanced Levoglucosan Yields from the Copyrolysis of Cellulose and High-Density Polyethylene. *ACS Sustainable Chem. Eng.* **2019,** *7,* 9480-9488, DOI 10.1021/acssuschemeng.9b00765.

7. Somoza-Tornos, A.; Gonzalez-Garay, A.; Pozo, C.; Graells, M.; Espuña, A.; Guillén-Gosálbez, G. Realizing the Potential High Benefits of Circular Economy the Chemical Industry: Ethylene Monomer Recovery via Polyethylene Pyrolysis. *ACS Sustainable Chem.Eng.* **2020,** *8,* 3561-3572, DOI 10.1021/acssuschemeng.9b04835.

8. Jeong, Y.; Park, K.; Kim, J. Hydrogen production from steam gasification of polyethylene using a two-stage gasifier and active carbon. *Appl. Energy* **2020,** *262,* 114495, DOI 10.1016/j.apenergy.2020.114495.

9. Wilk, V.; Hofbauer, H. Conversion of mixed plastic wastes in a dual fluidized bed steam gasifier. *Fuel* **2013,** *107,* 787-799, DOI 10.1016/j.fuel.2013.01.068.

10. Erkiaga, A.; Lopez, G.; Amutio, M.; Bilbao, J.; Olazar, M. Syngas from steam gasification of polyethylene in a conical spouted bed reactor. *Fuel* **2013,** *109,* 461-469, DOI 10.1016/j.fuel.2013.03.022.

11. He, M.; Xiao, B.; Hu, Z.; Liu, S.; Guo, X.; Luo, S. Syngas production from catalytic gasification of waste polyethylene: Influence of temperature on gas yield and composition. *Int. J. Hydrogen Energy* **2009,** *34,* 1342-1348, DOI 10.1016/j.ijhydene.2008.12.023.

12. Lopez, G.; Erkiaga, A.; Artetxe, M.; Amutio, M.; Bilbao, J.; Olazar, M. Hydrogen Production by High Density Polyethylene Steam Gasification and In-Line Volatile Reforming. *Ind. Eng. Chem. Res.* **2015,** *54,* 9536-9544, DOI 10.1021/acs.iecr.5b02413.

13. Namioka, T.; Saito, A.; Inoue, Y.; Park, Y.; Min, T. j.; Roh, S. a.; Yoshikawa, K. Hydrogen-rich gas production from waste plastics by pyrolysis and low-temperature steam reforming over a ruthenium catalyst. *Appl. Energy* **2011,** *88,* 2019-202, DOI 10.1016/j.apenergy.2010.12.053.

14. Chai, Y.; Gao, N.; Wang, M.; Wu, C. H2 production from co-pyrolysis/gasification of waste plastics and biomass under novel catalyst Ni-CaO-C. *Chem. Eng. J.* **2020,** *382,* 122947, DOI 10.1016/j.cej.2019.122947.

15. Kumagai, S.; Hosaka, T.; Kameda, T.; Yoshioka, T. Removal of toxic HCN and recovery of H2-rich syngas via catalytic reforming of product gas from gasification of polyimide over Ni/Mg/Al catalysts. *J. Anal. Appl. Pyrolysis* **2017,** *123,* 330-339, DOI 10.1016/j.jaap.2016.11.012.

16. Barbarias, I.; Lopez, G.; Alvarez, J.; Artetxe, M.; Arregi, A.; Bilbao, J.; Olazar, M. A sequential process for hydrogen production based on continuous HDPE fast pyrolysis and in-line steam reforming. *Chem. Eng. J.* **2016,** *296,* 191-198, DOI 10.1016/j.cej.2016.03.091.

17. Zhou, H.; Saad, J. M.; Li, Q.; Xu, Y. Steam reforming of polystyrene at a low temperature for high H2/CO gas with bimetallic Ni-Fe/ZrO2 catalyst. *Waste Manage.* **2020,** *104,* 42-50, DOI 10.1016/j.wasman.2020.01.017.

18. Nabgan, B.; Tahir, M.; Abdullah, T. A. T.; Nabgan, W.; Gambo, Y.; Mat, R.; Saeh, I. Ni/Pd-promoted Al2O3–La2O3 catalyst for hydrogen production from polyethylene terephthalate waste via steam reforming. *Int. J. Hydrogen Energy* **2017,** *42,* 10708-10721, DOI 10.1016/j.ijhydene.2017.02.034.

19. Yao, D.; Yang, H.; Chen, H.; Williams, P. T. Investigation of nickel-impregnated zeolite catalysts for hydrogen/syngas production from the catalytic reforming of waste polyethylene. *Appl. Catal. B* **2018,** *227,* 477-487, DOI 10.1016/j.apcatb.2018.01.050.

20. Bobek-Nagy, J.; Gao, N.; Quan, C.; Miskolczi, N.; Rippel-Pethő, D.; Kovács, K. Catalytic co-pyrolysis of packaging plastic and wood waste to achieve H2 rich syngas. *Int. J. Energy Res.* **2020**, DOI 10.1002/er.5741.

21. Al-Asadi, M.; Miskolczi, N. High temperature pyrolysis of municipal plastic waste using Me/Ni/ZSM-5 catalysts: The effect of metal/nickel ratio. *Energies* **2020,** *13,* 1284, DOI 10.3390/en13051284.

22. Al-asadi, M.; Miskolczi, N.; Eller, Z. Pyrolysis-gasification of wastes plastics for syngas production using metal modified zeolite catalysts under different ratio of nitrogen/oxygen. *J. Clean. Prod.* **2020,** *271,* 122186, DOI 10.1016/j.jclepro.2020.122186.

23. Lopez, G.; Artetxe, M.; Amutio, M.; Alvarez, J.; Bilbao, J.; Olazar, M. Recent advances in the gasification of waste plastics. A critical overview. *Renewable Sustainable Energy Rev.* **2018,** *82,* 576-596, DOI 10.1016/j.rser.2017.09.032.

24. Wu, C.; Williams, P. T. Pyrolysis-gasification of plastics, mixed plastics and real-world plastic waste with and without Ni-Mg-Al catalyst. *Fuel* **2010,** *89,* 3022-3032, DOI 10.1016/j.fuel.2010.05.032.

25. Park, Y.; Namioka, T.; Sakamoto, S.; Min, T. j.; Roh, S. a.; Yoshikawa, K. Optimum operating conditions for a two-stage gasification process fueled by polypropylene by means of continuous reactor over ruthenium catalyst. *Fuel Process. Technol.* **2010,** *91,* 951-957, DOI 10.1016/j.fuproc.2009.10.014.

26. Barbarias, I.; Lopez, G.; Artetxe, M.; Arregi, A.; Santamaria, L.; Bilbao, J.; Olazar, M. Pyrolysis and in-line catalytic steam reforming of polystyrene through a two-step reaction system. *J. Anal. Appl. Pyrolysis* **2016,** *122,* 502-510, DOI 10.1016/j.jaap.2016.10.006.

27. Saad, J. M.; Williams, P. T. Pyrolysis-Catalytic-Dry Reforming of Waste Plastics and Mixed Waste Plastics for Syngas Production. *Energy Fuels* **2016,** *30,* 3198-3204, DOI 10.1021/acs.energyfuels.5b02508.

28. Barbarias, I.; Lopez, G.; Artetxe, M.; Arregi, A.; Bilbao, J.; Olazar, M. Valorisation of different waste plastics by pyrolysis and in-line catalytic steam reforming for hydrogen production. *Energy Convers. Manage.* **2018,** *156,* 575-584, DOI 10.1016/j.enconman.2017.11.048.

29. Tsuji, T.; Hatayama, A. Gasification of waste plastics by steam reforming in a fluidized bed. *J. Mater. Cycles Waste Manage*. **2009,** *11,* 144-147, DOI 10.1007/s10163-008-0227-z.

30. Alvarez, J.; Kumagai, S.; Wu, C.; Yoshioka, T.; Bilbao, J.; Olazar, M. Hydrogen production from biomass and plastic mixtures by pyrolysis-gasification. *Int. J. Hydrogen Energy* **2014,** *39,* 10883-10891, DOI 10.1016/j.ijhydene.2014.04.189.

31. Arregi, A.; Amutio, M.; Lopez, G.; Artetxe, M.; Alvarez, J.; Bilbao, J.; Olazar, M. Hydrogen-rich gas production by continuous pyrolysis and in-line catalytic reforming of pine wood waste and HDPE mixtures. *Energy Convers. Manage.* **2017,** *136,* 192-201, DOI 10.1016/j.enconman.2017.01.008.

32. Barbarias, I.; Lopez, G.; Amutio, M.; Artetxe, M.; Alvarez, J.; Arregi, A.; Bilbao, J.; Olazar, M. Steam reforming of plastic pyrolysis model hydrocarbons and catalyst deactivation. *Appl. Catal., A* **2016,** *527,* 152-160, DOI 10.1016/j.apcata.2016.09.003.

33. Aminu, I.; Nahil, M. A.; Williams, P. T. Hydrogen from Waste Plastics by Two-Stage Pyrolysis/Low-Temperature Plasma Catalytic Processing. *Energy Fuels* **2020,** *34,* 11679-11689, DOI 10.1021/acs.energyfuels.0c02043.

34. Yao, D.; Yang, H.; Chen, H.; Williams, P. T. Co-precipitation, impregnation and so-gel preparation of Ni catalysts for pyrolysis-catalytic steam reforming of waste plastics. *Appl. Catal., B* **2018,** *239,* 565-577, DOI 10.1016/j.apcatb.2018.07.075.

35. Kumagai, S.; Yabuki, R.; Kameda, T.; Saito, Y.; Yoshioka, T. Simultaneous recovery of H2-rich syngas and removal of HCN during pyrolytic recycling of polyurethane by Ni/Mg/Al catalysts. *Chem. Eng. J.* **2019,** *361,* 408-415, DOI 10.1016/j.cej.2018.12.099.

36. Barbarias, I.; Artetxe, M.; Lopez, G.; Arregi, A.; Bilbao, J.; Olazar, M. Influence of the conditions for reforming HDPE pyrolysis volatiles on the catalyst deactivation by coke. *Fuel Process. Technol.* **2018,** *171,* 100-109, DOI 10.1016/j.fuproc.2017.11.003.

37. Wu, C.; Williams, P. T. Ni/CeO2/ZSM-5 catalysts for the production of hydrogen from the pyrolysis-gasification of polypropylene. *Int. J. Hydrogen Energy* **2009,** *34,* 6242-6252, DOI 10.1016/j.ijhydene.2009.05.121.

38. Wu, C.; Williams, P. T. Hydrogen Production from the Pyrolysis/Gasification of Polypropylene: Influence of Steam Flow Rate, Carrier Gas Flow Rate and Gasification Temperature. *Energy Fuels* **2009,** *23,* 5055-5061, DOI 10.1021/ef900278w.

39. Chai, Y.; Wang, M.; Gao, N.; Duan, Y.; Li, J. Experimental study on pyrolysis/gasification of biomass and plastics for H2 production under new dual-support catalyst. *Chem. Eng. J.* **2020,** *396,* 125260, DOI 10.1016/j.cej.2020.125260.

40. Chen, J.; Sun, J.; Wang, Y. Catalysts for Steam Reforming of Bio-oil: A Review. *Ind. Eng. Chem. Res.* **2017,** *56,* 4627-4637, DOI 10.1021/acs.iecr.7b00600.

41. Liu, L.; Zhang, Z.; Das, S.; Kawi, S. Reforming of tar from biomass gasification in a hybrid catalysis-plasma system: A review. *Appl. Catal., B* **2019,** *250,* 250-272, DOI 10.1016/j.apcatb.2019.03.039.

42. Nabgan, W.; Tuan Abdullah, T. A.; Mat, R.; Nabgan, B.; Gambo, Y.; Ibrahim, M.; Ahmad, A.; Jalil, A. A.; Triwahyono, S.; Saeh, I. Renewable hydrogen production from bio-oil derivative via catalytic steam reforming: An overview. *Renew. Sustain. Energy Rev.* **2017,** *79,* 347-357, DOI 10.1016/j.rser.2017.05.069.

43. Arregi, A.; Amutio, M.; Lopez, G.; Bilbao, J.; Olazar, M. Evaluation of thermochemical routes for hydrogen production from biomass: A review. *Energy Convers. Manage.* **2018,** *165,* 696-719, DOI 10.1016/j.enconman.2018.03.089.

44. Yung, M. M.; Jablonski, W. S.; Magrini-Bair, K. A. Review of catalytic conditioning of biomass-derived syngas. *Energy Fuels* **2009,** *23,* 1874-1887, DOI 10.1021/ef800830n.

45. Du, Z.; Zhang, Z.; Xu, C.; Wang, X.; Li, W. Lowerature Steam Reforming of Toluene and Biomass Tar over Biochar-Supported Ni Nanoparticles. *ACS Sustainable Chem. Eng.* **2019,** *7,* 3111-3119, DOI 10.1021/acssuschemeng.8b04872.

46. Artetxe, M.; Nahil, M. A.; Olazar, M.; Williams, P. T. Steam reforming of phenol as biomass tar model compound over Ni/Al2O3 catalyst. *Fuel* **2016,** *184,* 629-636, DOI 10.1016/j.fuel.2016.07.036.

47. Remiro, A.; Arandia, A.; Oar-Arteta, L.; Bilbao, J.; Gayubo, A. G. Regeneration of NiAl2O4 spinel type catalysts used in the reforming of raw bio-oil. *Appl. Catal., B* **2018,** *237,* 353-365, DOI 10.1016/j.apcatb.2018.06.005.

48. Nogueira, F. G. E.; Assaf, P. G. M.; Carvalho, H. W. P.; Assaf, E. M. Catalytic steam reforming of acetic acid as a model compound of bio-oil. *Appl. Catal., B* **2014,** *160-161,* 188-199, DOI 10.1016/j.apcatb.2014.05.024.

49. Charisiou, N. D.; Siakavelas, G.; Papageridis, K. N.; Baklavaridis, A.; Tzounis, L.; Avraam, D. G.; Goula, M. A. Syngas production via the biogas dry reforming reaction over nickel supported on modified with CeO2 and/or La2O3 alumina catalysts. *J. Nat. Gas Sci. Eng.* **2016,** *31,* 164-183, DOI 10.1016/j.jngse.2016.02.021.

50. Santamaria, L.; Artetxe, M.; Lopez, G.; Cortazar, M.; Amutio, M.; Bilbao, J.; Olazar, M. Effect of CeO2 and MgO promoters on the performance of a Ni/Al2O3 catalyst in the steam reforming of biomass pyrolysis volatiles. *Fuel Process. Technol.* **2020,** *198,* 106223, DOI 10.1016/j.fuproc.2019.106223.

51. Charisiou, N. D.; Papageridis, K. N.; Tzounis, L.; Sebastian, V.; Hinder, S. J.; Baker, M. A.; AlKetbi, M.; Polychronopoulou, K.; Goula, M. A. Ni supported on CaO-MgO-Al2O3 as a highly selective and stable catalyst for H2 production via the glycerol steam reforming reaction. *Int. J. Hydrogen Energy* **2019,** *44,* 256-273, DOI 10.1016/j.ijhydene.2018.02.165.

52. Valle, B.; Aramburu, B.; Benito, P. L.; Bilbao, J.; Gayubo, A. G. Biomass to hydrogen-rich gas via steam reforming of raw bio-oil over Ni/La2O3-AAl2O3 catalyst: Effect of space-time and steam-to-carbon ratio. *Fuel* **2018,** *216,* 445-455, DOI 10.1016/j.fuel.2017.11.151.

53. Kumagai, S.; Alvarez, J.; Blanco, P. H.; Wu, C.; Yoshioka, T.; Olazar, M.; Williams, P. T. Novel Ni-Mg-Al-Ca catalyst for enhanced hydrogen production for the pyrolysis-gasification of a biomass/plastic mixture. *J. Anal. Appl. Pyrolysis* **2015,** *113,* 15-21, DOI 10.1016/j.jaap.2014.09.012.

54. Wu, C.; Williams, P. T. Investigation of coke formation on Ni-Mg-Al catalyst for hydrogen production from the catalytic steam pyrolysis-gasification of polypropylene. *Appl. Catal., B.* **2010,** *96,* 198-207, DOI 10.1016/j.apcatb.2010.02.022.

55. Wu, C.; Williams, P. T. A novel Ni-Mg-Al-CaO catalyst with the dual functions of catalysis and CO2 sorption for H2 production from the pyrolysis-gasification of polypropylene. *Fuel* **2010,** *89,* 1435-1441, DOI 10.1016/j.fuel.2009.10.020.

56. Wu, C.; Williams, P. T. Hydrogen production from the pyrolysis-gasification of polypropylene: Influence of steam flow rate, carrier gas flow rate and gasification temperature. *Energy Fuels* **2009,** *23,* 5055-5061, DOI 10.1021/ef900278w.

57. Santamaria, L.; Arregi, A.; Lopez, G.; Artetxe, M.; Amutio, M.; Bilbao, J.; Olazar, M. Effect of La2O3 promotion on a Ni/Al2O3 catalyst for H2 production in the in-line biomass pyrolysis-reforming. *Fuel* **2020,** *262, 116593,* DOI 10.1016/j.fuel.2019.116593.

58. Santamaria, L.; Lopez, G.; Arregi, A.; Amutio, M.; Artetxe, M.; Bilbao, J.; Olazar, M. Stability of different Ni supported catalysts in the in-line steam reforming of biomass fast pyrolysis volatiles. *Appl. Catal., B* **2019,** *242,* 109-120, DOI 10.1016/j.apcatb.2018.09.081.

59. Asplund, M.; Calvin, J. J.; Zhang, Y.; Huang, B.; Woodfield, B. F. Heat capacity and thermodynamic functions of silica-doped γ-Al2O3. *J. Chem. Thermodyn.* **2018,** *118,* 165-174, DOI 10.1016/j.jct.2017.11.013.

60. Alvarez, J.; Amutio, M.; Lopez, G.; Bilbao, J.; Olazar, M. Fast co-pyrolysis of sewage sludge and lignocellulosic biomass in a conical spouted bed reactor. *Fuel* **2015,** *159,* 810-818, DOI 10.1016/j.fuel.2015.07.039.

61. Erkiaga, A.; Lopez, G.; Barbarias, I.; Artetxe, M.; Amutio, M.; Bilbao, J.; Olazar, M. HDPE pyrolysis-steam reforming in a tandem spouted bed-fixed bed reactor for H2 production. J. *Anal. Appl. Pyrolysis* **2015,** *116,* 34-41, DOI 10.1016/j.jaap.2015.10.010.

62. Osorio-Vargas, P.; Flores-González, N. A.; Navarro, R. M.; Fierro, J. L. G.; Campos, C. H.; Reyes, P. Improved stability of Ni/Al2O3 catalysts by effect of promoters (La2O3, CeO2) for ethanol steam-reforming reaction. *Catal. Today* **2016,** *259,* 27-38, DOI 10.1016/j.cattod.2015.04.037.

63. Mazumder, J.; de Lasa, H. I. Ni catalysts for steam gasification of biomass: Effect of La2O3 loading. *Catal. Today* **2014,** *237,* 100-110, DOI 10.1016/j.cattod.2014.02.015.

64. Nabgan, W.; Tuan Abdullah, T. A.; Mat, R.; Nabgan, B.; Gambo, Y.; Moghadamian, K. Acetic acid-phenol steam reforming for hydrogen production: Effect of different composition of La2O3-Al2O3 support for bimetallic Ni-Co catalyst. *J. Environ. Chem. Eng.* **2016,** *4,* 2765-2773, DOI 10.1016/j.jece.2016.05.030.

65. Sánchez-Sánchez, M. C.; Navarro, R. M.; Fierro, J. L. G. Ethanol steam reforming over Ni / Mx Oy-Al2 O3 (M = Ce, La, Zr and Mg) catalysts: Influence of support on the hydrogen production. *Int. J. Hydrogen Energy* **2007,** *32,* 1462-1471, DOI 10.1016/j.ijhydene.2006.10.025.

66. Wang, M.; Zhang, F.; Wang, S. Effect of La2O3 replacement on γ-Al2O3 supported nickel catalysts for acetic acid steam reforming. *Int. J. Hydrogen Energy* **2017,** *42,* 20540-20548, DOI 10.1016/j.ijhydene.2017.06.147.

67. Sánchez-Sánchez, M. C.; Navarro, R. M.; Fierro, J. L. G. Ethanol steam reforming over Ni/La–Al2O3 catalysts: Influence of lanthanum loading. *Catal. Today* **2007,** *129,* 336-345, DOI 10.1016/j.cattod.2006.10.013.

68. García-García, I.; Acha, E.; Bizkarra, K.; Martínez de Ilarduya, J.; Requies, J.; Cambra, J. F. Hydrogen production by steam reforming of m-cresol, a bio-oil model compound, using catalysts supported on conventional and unconventional supports. *Int. J. Hydrogen Energy* **2015,** *40,* 14445-14455, DOI 10.1016/j.ijhydene.2015.07.155.

69. Santamaria, L.; Lopez, G.; Arregi, A.; Amutio, M.; Artetxe, M.; Bilbao, J.; Olazar, M. Influence of the support on Ni catalysts performance in the in-line steam reforming of biomass fast pyrolysis derived volatiles. *Appl. Catal., B* **2018,** *229,* 105-113, DOI 10.1016/j.apcatb.2018.02.003.

70. Navarro, R. M.; Guil-Lopez, R.; Ismail, A. A.; Al-Sayari, S. A.; Fierro, J. L. G. Ni- and PtNi-catalysts supported on Al2O3 for acetone steam reforming: Effect of the modification of support with Ce, la and Mg. *Catal. Today* **2015,** *242,* 60-70, DOI 10.1016/j.cattod.2014.07.036.

71. Valle, B.; Aramburu, B.; Remiro, A.; Bilbao, J.; Gayubo, A. G. Effect of calcination/reduction conditions of Ni/La2O3-Al2O3 catalyst on its activity and stability for hydrogen production by steam reforming of raw bio-oil/ethanol. *Appl. Catal., B* **2014,** *147,* 402, DOI 10.1016/j.apcatb.2013.09.022.

72. International Centre for Diffraction Data. **2003**.

73. Navarro, R. M.; Álvarez-Galván, M. C.; Rosa, F.; Fierro, J. L. G. Hydrogen production by oxidative reforming of hexadecane over Ni and Pt catalysts supported on Ce/La-doped Al2O3. *Appl. Catal., A* **2006,** *297,* 60-72, DOI 10.1016/j.apcata.2005.08.036.

74. Bizkarra, K.; Bermudez, J. M.; Arcelus-Arrillaga, P.; Barrio, V. L.; Cambra, J. F.; Millan, M. Nickel based monometallic and bimetallic catalysts for synthetic and real bio-oil steam reforming. *Int. J. Hydrogen Energy* **2018,** *43,* 11706-11718, DOI 10.1016/j.ijhydene.2018.03.049.

75. Yamamoto, T.; Hatsui, T.; Matsuyama, T.; Tanaka, T.; Funabiki, T. Structures and Acid-Base Properties of La/Al2O3 Role of La Addition to Enhance Thermal Stability of Al2O3. *Chem. Mater.* **2003,** *15,* 4830-4840, DOI 10.1021/cm034732c.

76. Predel, M.; Kaminsky, W. Pyrolysis of mixed polyolefins in a fluidized-bed reactor and on a pyro-GC/MS to yield aliphatic waxes. *Polym. Degrad. Stab.* **2000,** *70,* 373-385, DOI 10.1016/S0141-3910(00)00131-2.

77. Takuma, K.; Uemichi, Y.; Ayame, A. Product distribution from catalytic degradation of polyethylene over H-gallosilicate. *Appl. Catal. A* **2000,** *192,* 273-280, DOI 10.1016/S0926-860X(99)00399-3.

78. Williams, P. T.; Williams, E. A. Fluidised bed pyrolysis of low density polyethylene to produce petrochemical feedstock. *J. Anal. Appl. Pyrolysis* **1999,** *51,* 107-126, DOI 10.1016/S0165-2370(99)00011-X.

79. Czernik, S.; French, R. J. Production of hydrogen from plastics by pyrolysis and catalytic steam reform. *Energy Fuels* **2006,** *20,* 754-758, DOI 10.1021/ef050354h.

80. Cao, J.; Liu, T.; Ren, J.; Zhao, X.; Wu, Y.; Wang, J.; Ren, X.; Wei, . Preparation and characterization of nickel loaded on resin char as tar reforming catalyst for biomass gasification. *J. Anal. Appl. Pyrolysis* **2017,** *127,* 82-90, DOI 10.1016/j.jaap.2017.08.020.

81. Yu, H.; Liu, Y.; Liu, J.; Chen, D. High catalytic performance of an innovative Ni/magnesium slag catalyst for the syngas production and tar removal from biomass pyrolysis. *Fuel* **2019,** *254,* 115622, DOI 10.1016/j.fuel.2019.115622.

82. Santamaria, L.; Lopez, G.; Arregi, A.; Amutio, M.; Artetxe, M.; Bilbao, J.; Olazar, M. Effect of calcination conditions on the performance of Ni/MgO-Al2O3 catalysts in the steam reforming of biomass fast pyrolysis volatiles. *Catal. Sci. Technol.* **2019,** *9,* 3947-3963, DOI 10.1039/c9cy00597h.

83. Garcia, L.; French, R.; Czernik, S.; Chornet, E. Catalytic steam reforming of bio-oils for the production of hydrogen: effects of catalyst composition. *Appl. Catal., A* **2000,** *201,* 225-239, DOI 10.1016/S0926-860X(00)00440-3.

84. Salehi, E.; Azad, F. S.; Harding, T.; Abedi, J. Production of hydrogen by steam reforming of bio-oil over Ni/Al2O3 catalysts: effect of addition of promoter and preparation procedure. *Fuel Process. Technol.* **2011,** *92,* 2203-2210, DOI 10.1016/j.fuproc.2011.07.002.

85. Argyle, M. D.; Bartholomew, C. H. Heterogeneous catalyst deactivation and regeneration: A review. *Catalysts* **2015,** *5,* 145-269, DOI 10.3390/catal5010145.

86. Bartholomew, C. H. Mechanisms of catalyst deactivation. *Appl. Catal., A* **2001,** *212,* 17-60, DOI 10.1016/S0926-860X(00)00843-7.

87. Zhang, R.; Wang, Y.; Brown, R. C. Steam reforming of tar compounds over Ni/olivine catalysts doped with CeO2. *Energy Convers. Manage.* **2007,** *48,* 68-77, DOI 10.1016/j.enconman.2006.05.001.

88. Matas Güell, B.; Babich, I. V.; Lefferts, L.; Seshan, K. Steam reforming of phenol over Ni-based catalysts – A comparative study. *Appl. Catal., B* **2011,** *106,* 280-286, DOI 10.1016/j.apcatb.2011.05.012.

89. Zhang, F.; Wang, M.; Zhu, L.; Wang, S.; Zhou, J.; Luo, Z.A comparative research on the catalytic activity of La2O3 and γ-Al2O3 supported catalysts for acetic acid steam reforming. *Int. J. Hydrogen Energy* **2017,** *42,* 3667-3675, DOI 10.1016/j.ijhydene.2016.06.264.

90. Chen, J.; Sun, J.; Wang, Y. Catalysts for Steam Reforming of Bio-oil: A Review. *Ind. Eng. Chem. Res.* **2017,** *56,* 4627-4637, DOI 10.1021/acs.iecr.7b00600.

91. Chen, W.; Zhao, G.; Xue, Q.; Chen, L.; Lu, Y. High carbon-resistance Ni/CeAlO3-Al2O3 catalyst for CH4/CO2 reforming. *Appl. Catal., B* **2013,** *136-137,* 260-268, DOI 10.1016/j.apcatb.2013.01.044.

92. Trane-Restrup, R.; Jensen, A. D. Steam reforming of cyclic model compounds of bio-oil over Ni-based catalysts: Product distribution and carbon formation. *Appl. Catal., B* **2015,** *165,* 117-127, DOI 10.1016/j.apcatb.2014.09.026.

For Table of Contents Use Only

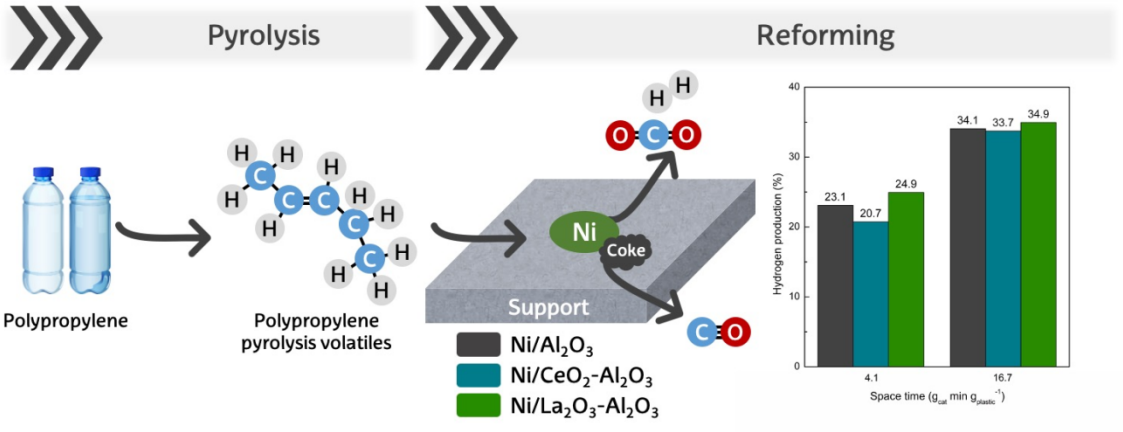

Waste polypropylene was selectively converted to hydrogen using different Ni promoted catalysts in a continuous pyrolysis reforming process